Tectonics Along the Himalayan and Andean Mountain Ranges: Numerical Analyses of Collision and Subduction Zones

Nedoma, Jiří
2007

Institute of Computer Science
Academy of Sciences of the Czech Republic

Tectonics Along the Himalayan and Andean Mountain Ranges: Numerical Analyses of Collision and Subduction Zones

Jiří Nedoma

Technical report No. 1011

December 2007

Pod Vodárenskou věží 2, 182 07 Prague 8, phone: +420 266 051 111, fax: +420 286 585 789,
e-mail:nedoma@cs.cas.cz

Institute of Computer Science
Academy of Sciences of the Czech Republic

Tectonics Along the Himalayan and Andean Mountain Ranges: Numerical Analyses of Collision and Subduction Zones

Jiří Nedoma

Technical report No. 1011

December 2007

Abstract:

To investigate the upper lithospheric structure, subduction-inducted and collision-induced processes across the Andes, the Andaman-Nicobar Island Arc system and the Himalayas the numerical models will be used and discussed. The models will be based on the plate tectonic hypothesis, the multibody contact theory and the finite element method. The distributions of the interplate stress-strain rates as well as the convergence rates and the normal and tangential contact stress rates in the investigated areas will be discussed.

Keywords:
Geodynamics, mathematical modelling, Andes, Himalayas, Andaman Arc system, contact problems, finite element method

1 Introduction

To analyze geological, tectonic and geodynamic processes in subduction and collision zones the earth sciences as well as mathematical modelling are usually used. We will distinguish between fast and slow geological processes. The rate of processes began to be compared, and which were faster and which slower began to be determined. Then the earth sciences have deducted to a degree that it is necessary to know how many millimeters a mountain range has risen or has subsided over the year. Crustal movements are usually a combination of horizontal and vertical movement components. Tectonic movements do not usually display a constant and regular character, but have an episodic character (Doglioni et al. (1999), Lister et al. (2001)). Rapid movements alternate with longer periods of relative inactivity. From the point of view of longer durations of movements the average rates of movements are smaller than for the case of smaller movement durations.

Orogenesis is a long-term process, and therefore, it is difficult to compare its rate with the rates of recent crustal movements. Classical regions of young uplifts are some tectonically active areas as the collision of the Indian plate with the Eurasian plate and/or the subduction of the Nazca plate beneath the South American plate. In the Himalayas the mountain ranges have usually been elevated by $5-6km$, in the main world orogenesis and in the Andes by $2-4km$ above the surrounding landscape, which corresponds to the average rate of orogenesis to be $0.7-0.8mm.a^{-1}$ over the last $25Ma$ in the Himalayas (Mehta, 1980) or $0.6mm.a^{-1}$ in the main world orogenesis and in the Andes (Spencer, 1974).

The collision of lithosperic plates represents the actual cause of the large stresses and strains in the lithosphere. The lithosphere thus behaves like a stress guide. Since this process plays an important role in tectonophysics, therefore, we will study this problem in more details in several cases - subductions of the Nazca plate beneath the South American plate and of the Indian plate beneath the Barma plate and the collision of Indian plate with the Eurasian plate.

To understand of tectonics of these active regions, the mathematical modelling of deformation and stress fields can be preferably used, and namely, the numerical modelling is one of effective techniques for analysing the seismotectonics in areas of our interests. The finite element method is useful for such calculations. Firstly this method, based on the approach of classical BVPs, was used for analyses of deformations and stresses in the Himalayas and the Tibetan Plateau. Several authors as Sato et al. (1996), and others, applied the so-called roller conditions, where only the displacements parallel to the boundaries are allowed. These types of model problems do not allow to study the active deep faults in the investigated region as the MBT, MCT, etc., faults. In these models all active faults are actually approximated not as active faults but as "sutures". Moreover, these type of models do not allow to investigate time periods greater then $100yrs$. Sizable difficulties of the roller type conditions are in the fact that the prescribed displacements on the boundary (distributions of which are not known) strongly influence the distributions of displacement, strain and stress fields in the investigated region upto great distances from these boundaries.

All the above discussed difficulties can be removed introducing the theory of multibody contact problems (see Nedoma (1987), (1990a,b), (1998a)) as the movements of invasing plates are known and can be determined in the defined distances from the collision and the subduction zones. The useful data can be obtained from the geological, geophysical and/or from the satellite observations. In contrast to the above discussed models with roller conditions the models based on the multibody contact theory minimize the functional of potential energy not over the space of virtual displacements (as it was in the previous models) but over the set of admissible displacements determined by the condition of nonpenetration and for time period less than $1.2 \times 10^5 yrs$, i.e. for time periods much more higher than in the previous models with roller conditions.

In this contribution we will analyze and then will discuss the tectonics in the Himalayan collision zone and in the subduction zone of the Andaman arc system and in the Andean subduction zone. The nature of the collision between the Indian and Eurasian plates in the Himalayan region as well as in the Andaman Island Arc system, and moreover, the nature of the subduction of the Nazca plate beneath the South American plate, have been investigated by using the mathematical modelling based on the theory of multibody contact problems. We will assume that all physical data do not depend on the x_2-coordinate.

2 Evolution of tectonics of the upper parts of the Earth

The seismicity in the Earth's lithosphere is usually explained by tectonic stresses, accompanied also by crustal movements. The regions with strong seismicity are areas of continental episodic displacements, upthrusts and downthrusts. Fast movements alternate with quiet periods and depend on geological processes taking place in the deeper parts of the Earth below the lithosphere (Doglioni et al. (1999), Nedoma (1998a)). The hypothesis which is most probable at this time is that of tectonics of lithospheric plates - plate tectonics. Plate tectonics is a hypothesis explaining tectonic and seismic activity in the upper parts of the Earth by operation of several large lithospheric plates and several tens of smaller geological blocks into which the upper part of the Earth is broken. The term lithosphere relates to the outer solid upper part of the Earth, broken into blocks and greater plates, moving on the underlaying asthenosphere. The thickness of the lithosphere is of about $80 - 100km$ on average. The asthenosphere is a layer below the lithosphere, characterized by lower velocities of seismic waves and lower viscosity. Boundaries between geological blocks and plates are situated within active seismic zones, where most of the mechanical energy is being consumed, and are of the divergent, transform and convergent types. Convergent boundaries, which will be of our interest in this paper, occur in sites of oceanic lithospheric consumption - subduction zones, and in those of continental lithospheric collision. Subduction zones are accompanied by intense seismicity in the so-called Wadati-Benioff zones, in which more than 85% of seismic energy is consumed. Continental collisions represent a final stage of the evolution of convergent plate boundaries, characterized by the Alpides - the Alpine-Himalayan mountain belt (Doglioni et al. (1999). Both types of convergent boundaries can occur during the evolution process like the evolution of the Himalayan mountain arc (see Fig.1), where during the first part of evolution the Tethyan oceanic lithosphere is subducted and the Tibetan plato originates and during the second period of evolution the collision of the continental parts of the plates (the Indian subcontinent and the Eurasian plate) cannot be consumed because of their considerable thickness. This is the reason why we will also investigate the subduction Andean zone. Our investigation will be based on the theory of multibody contact problems, which moreover, admits to clear up the mechanism of earthquakes in these studied regions (Nedoma (1987),(1990a-c),(1998a).

2.1 Seismotectonics of Andes and the plate tectonic model

The Andean region is located in one of the most seismically active regions in the world, where the responsible process is the subduction of the Nazca plate underneath the South American plate along the Peru-Chile trench since the Cretaceous. It is the largest region between $10°N$ and $43°S$ in which ocean-continent convergence is the present event. The present relief of the Andes has developed in the past 10 to $20Myrs$, while the subduction of the oceanic plate below the continental South America had the origin $\sim 140 - 200Myrs$ ago. The continental margin orogenic belt is more than $7000km$ length. The magmatism associated with the subduction zone of South America is calc-alcaline to high-K calc-alcaline. Na-alcaline volcanoes are also present in some areas such as various sectors of the eastern margin of South America where they occur as scattered centers east of the calc-alcaline volcanic belt (Doglioni et al. (1999)). The chemical properties of volcano rocks depend on the depth of magma deposits (Nedoma (1998a)). Along the Peru-Chile trench, the subduction of the Nazca Plate under the South American Plate is well characterized by the Wadati-Benioff zone (WBZ), which has been frequently studied by using the seismic activity (Figs 2a,b,c) and the plate tectonic hypothesis. Barazangi, Isacks (1976), Rodrigues, Tavera (1991), Berrocal, Fernandes (1996), indicate the existence of specific features in the Nazca slab beneath the Andean region, namely the changes of the WBZ dip. Between $\sim 17°S - 25°S$ the Nazca plate dips eastward below the continent with an angle $\sim 25 - 30°$, southward and also northward the angle of subduction decreases.

The WBZ beneath the southern Peru and the northern Chile region was analyzed by Hasegawa, Sacks (1981), Grange et al. (1984), Boyd et al. (1984), Barazangi, Isacks (1976). Comte, Suarez (1994), Comte et al. (1994) indicate phase transformation along the slab with normal and reverse faulting at around $100km$ and $200km$ of depth and the existence of subducted oceanic crust. Delouis et al. (1996) determined a WBZ with a seismically coupled plate interface and localized reverse faults among $20 - 30km$ of depth. The seismic activities between $70 - 300 - 500km$ of depth and the concentration of the deep earthquakes in relatively narrow zones oriented almost in the $N - S$ direction

give important information for determination of mechanical properties and for the stress distribution of the descending slab. A fundamental problem in seismology represents determination of the mechanism of very deep earthquakes. Important contraversies exist about the seismotectonic characteristics in the Andean region, in relation both to the morphology of the Wadati-Benioff zone (WBZ) and to the focal mechanism responsible for the very deep ($h > 500km$) South American earthquakes (Cahill, Isacks (1992), Berrocal, Fernandes (1996), (2005)). In their study the Andean region was divided into groups of cross-sections investigating the WBZ and characterized by 13 transversal sections S1, ..., S13. They show the WBZ dipping to the East, with the hypocentres projected into vertical planes, that are oriented almost perpendicular to the oceanic trench. In the maps of these profiles the epicentral areas corresponding to each section are presented. In Fig.2a the epicentres of events with $h \leq 50km$, including shallow activity belonging to the beginning of the WBZ, close to the Peru-Chile oceanic trench and to activity in the continental crust of western South America are presented, while in Fig.2b are presented the earthquakes with $h > 50km$, to include mainly the activity in the WBZ beneath the Andean region among $0°$ and $50°S$. In Fig.2c the longitudinal $S-N$ section to the Andean region is presented. Figs 2a,b,c permit to define the important seismotectonic features and permit to suggest lateral and in depth correlations between shallow and intermediate depth seismotectonic activity with the very deep earthquakes beneath the Andean region. The WBZ among $35°S$ and $27.5°S$ indicates two continuous levels of high rate of seismic activity, the first one from the surface to $\sim 75km$ of depth and other from $\sim 100km$ to $125km$ of depth. A clear gap of intermediate depth earthquakes between $70km$ and $300km$ are situated North of $27.5°S$. This gap extended up to around $26°S$, with almost no earthquakes in that range of depths, and up to $24.5°S$ for intermediate depth earthquakes below $100km$. The characteristics of the shallower WBZ clearly change to the North of $24.5°S$, where the seismic activity gets deeper, going rapidly from $150km$ to $300km$ of depth at $22°S$. The block of the shallower WBZ, situated from $24.5°S$ beneath northern Chile and southern Peru, is extended up to latidude $14.5°S$ and seems to correlate well in depth with deep earthquakes located in northern Argentina and southern Bolivia. Northwards than $14.5°S$ there is a sudden reduction in the WBZ depth from $250km$ to $100km$ that increases again up to $150km$ beneath $9°S$. This gap of intermediate depth activity, below $100-150km$, may be related to the subduction of the Nazca ridge. Among the latidute $9°S$ to $1°S$ the WBZ is located beneath northern Peru and southern Ecuador and is characterized by two levels of seismic activity. The first level of seismic activity corresponds to the beginning of the Nazca plate subduction and to the continental crust earthquakes. The second one corresponds to the flat WBZ existent in this region with its upper surface in depth between $100km$ to $125km$. The northern extreme shallower events could be correlated with the northern extreme very deep earthquakes in the Peru-Brazil region. For more details see Engdahl et al. (1995), (1997), Berrocal, Fernandes (1996a,b).

To analyze the tectonics in the Andean region we will construct two models based on the profile $S2$ across the Villarica volcano and on the profile $S10B$ across the Peru-Chile border, determined from the results of Berrocal, Fernandes (1996) and Engdahl et al. (1997), Berrocal et al. (2000) (see Figs 3a,b). The geometry of the models is based on the determination of epicenters of earthquakes and on the shape of the WBZ (Fig.3a,b) as well as on the analyses of deep faults together with a spatial distribution of volcanoes (Fig.4).

2.2 Seismotectonics of Himalayan and Andaman Arc regions and the plate tectonic models

The Himalayas and the Andaman Island Arc system are products of continent/ continent collision between the Indian and the Eurasian plates in the first case and of subduction of the Indian plate beneath the Burmese plate in the second one and represent one of the most active collision zones in the world (Verma (1991b), DasGupta et al. (2003)). Paleomagnetic studies show (Klootwijk (1979), Aitchison et al. (2007)) that the India lay very much south of the equator and started to moving northward around $140Ma$. During the Mesozoic and the Early Tertiary an ocean basin (the Tethys basin) lay between the India and the rest of Eurasia. The oceanic (Tethyan) part after moving India to the north was divided by a deep fault between the Indian and Eurasian plates. In the next stage of the evolution the Tethyan plate subducted below the Eurasian plate with different velocities and started to collide with the Eurasian plate sometime during the Miocene. Results of Nedoma (1986),

(1990a,b,c), (1998a,b) indicate a deep fault originated in the oceanic (Tethyan) lithosphere near the pre-Eurasian plate, which during the whole evolution process will be the main contact boundary between the invasing Indian plate and the pre-Eurasian plate. Since the speed of the invasing Indian plate was approx. $18cm/yr$ (similarly as at present in the subduction zone of the Nazca plate approx. $10cm/yr$) the Indian plate sank below the Eurasian plate. When the speed of the invasing plate was less than $8cm/yr$ the Tibetan Arc system started to originate. The further stage of evolution was represented by the situation when the invasing Indian plate pressed the Tibetan arc system. Since the first contact of the invasing Indian plate with the Eurasian plate was in the Nanga Parbat region, then the Karakoram was originated, the invasing Indian plate rotated and as a result of the further collision the Tibetan Plateau and the Himalayan Arc system were originated accompanying with the new system of deep faults. According to them the High Himalayas have been uplifted as a result of major thrust sheets. As a result of the thrust movements Paleozoic and Mesozoic sediments deposited in the Tethyan basin were folded and uplifted resulting in the formation of High Himalayas. Later Makovsky et al. (1996) introduced three versions of the geodynamical model of the Himalayas, using the results of the INDEPTH project in the Himalayan-Tibetan region, where the third version of the model seems to correspond with a certain probability to upper parts of the lithosphere. Aitchison et al. (2007) on the basis of new field evidence from Tibet and of published papers suggest that continent-continent collision began around the Eocene/Oligocene boundary ($\sim 34Ma$) and propose an alternative explanation for events at $55Ma$. Crouzet et al. (2003) from paleomagnetic studies suggest that the main Himalayan folding is older than $35Ma$ in the western Dolpo area (Tethyan Himalaya, Nepal) and that a clockwise rotation of $10-15°$ is inferred from the pyrrhotite and magnetide components, but indicating that no rotation of the Tethyan Himalayan relative to India took place before $35Ma$. The mechanism of the Eocene/Oligocene Alpine orogen was studied by Doglioni et al. (1999), which is in a good agreement with results of Nedoma (1998a,b) concerning the mechanism of Himalayan evolution, based on the plate tectonic hypothesis, the multibody contact theory and the finite element method, where numerically the frontal thrust belt and the back thrust belt are also observed.

The Himalayan region is created by the sub-Himalayas (the Siwalik belt), the Lesser and High Himalayas and the Tibetan Plateau (see Fig.5a). The Himalayan Arc is of about 2500km long and of about 200-250km wide. The Andaman Island Arc region is situated in northeastern part of the Indian ocean and is formed by the young sedimentary rocks. Together with the Burmese arc it creates a 2200km long arc of the subduction zone of the Indian plate beneath the Burmese plate. The active subduction is documented by the active Barren-Narcondam volcanism. Major tectonic elements are the Andaman Trench, the Andaman-Nicobar Ridge, the Nicobar Deep, the West Andaman Fault, the Andaman Sea and the Mergui Terrace (see Fig. 5b, Fig. 6b).

Detailed seismicity along the Himalayan arc and the Andaman Arc system, in a dependence on the tectonics of these regions, has been discussed by Rastogi (1974), Armbruster et al. (1978), Verma et al. (1978), Quittmeyer and Jacob (1979), Ni and Barazangi (1984), Valdyia (1984), Verma and Kumar (1987), Mukhopadhyay and DasGupta (1988), Molnar (1990), Verma (1991a,b), Chandra (1992), Mukhopadhyay (1984), (1992), Radha, Sanu (2002), DasGupta et al. (2003), Ramesh (2005), Mitra et al. (2005), Monsalve et al. (2006), Copley, McKenzie (2007) and several others. A seismicity map of the western Himalayan arc (from 27° to $36°N$, 70° to $82°E$) is shown in Fig.6a, while Fig.6b shows the seismicity along the eastern part of the arc (extending from 86° to $97°E$, 22° to $30°N$). Data for these were compiled and are presented by Verma (1991b), Mukhopadhyay (1984).

Most of the events of mag. 6.0 and more are located close to the Main Central Thrust (MCT). Focal mechanism studies show that most of the events have resulted due to thrust faulting at a depth of 12-20km, which suggests underthrusting of the Indian shield underneath the High/Tethys Himalayas (Verma and Kumar (1987); Ni and Barazangi (1984)). Ni and Barazangi (1984) and Powell and Conagham (1973) have proposed models suggesting that the Indian continental crust underthrusts the Tethys slab and generates large magnitude earthquakes near the MBF/MBT and major earthquakes near the MCT. In the area between the MBT and the MCT there are other deep faults which are also active.

Numerical modelling represents one of effective way how to solve the problem. For models with different rheologies numerical methods were applied by some workers (Vilotte et al. (1986); Wang et al.

(1982); Zhao and Morgan (1985); Chander et al. (1986); Sato et al. (1996), Nedoma (1998a,b), Berger et al. (2004), etc.). The underthrusting model is strongly supported by results obtained from the project INDEPTH carried out in the High Himalayas/Tibetan Plateau region (see Nelson et al. (1996), Brown et al. (1996), Makovsky et al. (1996)). They interpreted the results of the INDEPTH project as the evidence of existence of the Main Himalayan Thrust (MHT), which dips norward underneath the Lesser as well as the High Himalayas and the Kangman Dome in Tibet (Zhao et al. (1993)). The MBT and the MCT merge with this thrust. Berger et al. (2004) analysed the structure of the Himalayas in Nepal along the MHT. They estimate the influence of the topography, the geometry of the flat-ramp-flat transition of the MHT and its rheology as well as the active deformation of Nepal, i.e. neotectonics, microseismicity, GPS velocity, vertical displacement rates. They suggest a small amount of aseismic slip along the southern part of MHT and an abrupt change in geometry of the MHT between Central and Western Nepal. Solon et al. (2005) from the INDEPTH magnetotelluric data indicated the double thickness crust. Guoyn Ding et al. (2004) imply northeastward dimishing of the total horizontal displacement and temporal getting younger of the fault slip along the northern margin of the Tibetan Plateau (NMTP) - a major intracontinental Cenozoic transpressional zone that comprises a series of active strike-slip faults and thrust faults.

To understand tectonics of these regions, the mathematical models based on the plate-tectonic hypothesis, the theory of multibody contact problems and the finite element method, will be used. It is evident that the mathematical simulation of the evolution of the northern part of Indian Ocean region must be described by the same type of mathematical models as the collision Himalayan zone and the subduction Andaman-Nicobar Islands-Sumatra Arc system are situated in one bigger region. Thus their corresponding models must follow from the geodynamical model of evolution of the previous stage, where the geometry and physical parameters change in time only. Based on the plate tectonic hypothesis and the multibody contact theory the frontal thrust belt and the back thrust belt were numerically verified (Nedoma (1998a,b)).

2.3 Discussion of results

Analyses of seismotectonic features of the WBZ in the Andean region

The obtained results were based on the analyses of the spatial distribution of high quality of earthquake hypocentres (based on data during January 1964-December 1995), published in Berrocal, Fernandes (1996) (see Figs 3a,b). In this study we analyze sections S2 and S10B. Section S2 represents the profile across the Villarica volcano and we see the WBZ with a dip of around 20° and a maximum depth of $150km$ and at a distance of less than $200km$ from the trench (denoted by the symbol $\Downarrow$). The profile S10B - the profile at Peru-Chile border, represents the WBZ with seismic activity up to $300km$ of depth, followed by a seismic gap up to $550km$ and then it continuous with the very deep activity up to of around $600km$ of depth. Section S10B seems to be a best representation of the WBZ in the Andean region (Berrocal et al. (2000)).

In our approach we will assume that the present relative movements of the Nazca plate is approx. $10cm/yr$ and that all geophysical data do not depend on the x_2-axis. The present relative movements of the South American Plate in its central part is observed of about $2.5cm/yr$. In our study we will investigate the behaviour of the upper parts of the Earth during very short (from the geological point of view) geological time period and we will assume that the investigated geological time interval is a sum of time intervals, which are shorter than the so-called characteristic time for which the lithosphere behaves as an elastic medium; for longer geological time periods it behaves as a visco-elastic medium. The models, based on the profiles S2 and S10B, assume the lithospheric plates of $80 - 100km$ thick, with densities between $2500 - 3400kgm^{-3}$, velocities of seismic P-waves between $6100 - 8120m\,\mathrm{sec}^{-1}$ and velocities of seismic S-waves between $3540 - 4690m\,\mathrm{sec}^{-1}$. The geometry configuration was obtained from the distribution of intermediate and deep earthquakes as well as of deep faults locations. Furthermore, we assume that the Earth surface is load free and that the invazing Nazca plate moves during the investigated time period by an uniform velocity. The lithosphere is modelled by a non-homogeneous and broken up medium resting on the asthenosphere. On contact

boundaries between geological blocks into which the lithosphere is broken up as well as on the contact boundary between the lithosphere and the asthenosphere the friction of Coulombian type is assumed.

The main results are illustrated in Figs 7-10 for the relatively short geological time period. In Fig.7 the geometry of the model problem corresponding to the profile S2 across the volcano Villarica is presented. In Figs 8a-d the interplate stresses in MPa and the principal stresses (where $\longrightarrow\longleftarrow$ denotes pressures, $\longleftarrow\longrightarrow$ denotes tension stresses) are presented, while in Figs 8e-i the normal and tangential contact stresses and displacements at the contact boundaries (denoted as Tn, Tt, DUn, DUt) and the rate of uplifts are illustrated. From the graph of normal contact displacements DUn we indicate areas in the subduction zone with nonzero DUn (Fig.8h), while between the South American lithospheric plate and the asthenosphere we indicate areas with $DUn = 0$ (Fig.8i). Temperature of rock melting depends on the pressure and the temperature. If the pressure increase the temperature of melting also increases, if it decreases then the temperature of melting also decreases. On the contact boundaries the Signorini type of contact conditions are prescribed. Then since the pressure decreases in the areas when the normal component of displacement vector is nonzero, the rocks are melted or partially melted, resulting in these areas the volcano chambers. We can indicate the volcanic chamber of the volcano Villarica in the depth of about $50km$. The graph of DUn describes the size and the shape of volcanic chambers originated during the investigated time interval. The tangential component of displacements DUt characterizes the mutual movements of the lithosperical blocks at the contact boundaries. Fig.8i illustrates the facts that between contact points (39,17,53) $DUn = 0$, i.e. both plates are in a contact, and DUt indicates that the shift of the invasing plate as well as the rate of its velocity during the investigated time period rapidly decrease in the direction to the East. The tensile stresses indicated in Fig.8d characterize the places where the deep faults are observed. Fig.8g illustrates the rate of interplate vertical component of displacement vector (i.e. the rate of uplift in $[mm/yr]$), where we can observe the areas of greater values of vertical component of displacement vector, corresponding to the bulged out areas and areas with great seismic and volcanic activities. Moreover, we can observe the rate of uplifts, building the forearc, and the rate of subsidence in the place where the oceanic crust descends below the continental lithosphere, building the Peru-Chile Trench. Since during the evolution rocks absorbed gases, then the gases after their release from the melted rocks compress the magma and transport it along these deep fault up to the Earth surface, where the volcano Villarica, and in relatively small vicinity, the volcanoes Quetrupillán and Lanín are situated. In Figs.8e,f the distribution of normal and tangential contact stresses are illustrated, where we can observed areas with great pressures and tensile stresses. Our numerical results indicate for the Villarica volcano profile maximal stresses in the region of about $50km$ depth, where great tensions and compressions in the Wadati-Benioff zone with maximal tensions at the depth approx. $55 - 65km$ are indicated. From the contact conditions the mechanism of earthquake follows immediatelly. Due to the forces acting on both plates and the friction forces acting on the contact boundaries, the following two cases can occur. Firstly, if the absolute value of the tangential contact stresses acting in the contact zone is less than the frictional forces then the tangential force precludes the mutual motion of both colliding plates and blocks and in this area the deformation energy henceforth cumulates. Secondly, if the absolute value of tangential contact stresses is equal to the friction force, then there are no forces which can preclude the mutual motion of both plates. The contact points change their positions in the direction opposite to that in which the tangential contact stresses act, and moreover, one part of the accumulated energy is emanated as an earthquake (see Nedoma (1998a)).

In Fig. 9 the geometry of the model corresponding to the profile S10B - the Peru/Chile border, is presented. In Figs 10a-d the rate of principal stresses in the whole investigated region and the rate of interplate horizontal, shear and vertical stresses are given. Analysing these results we eliminate places where stresses are accumulated; the first one is situated at the depth of about $22km$ and in distance approx. $42km$ from the Peru/Chile trench; the second one is situated at the depth of about $175km$ and in distance from the Peru/Chile trench of about $330km$ and the third one at the depth of about $590km$ and in the distance from the Peru/Chile trench of about $1000km$, where the maximal compression is observed. In the depth of about $610km$ and the distance from the Peru/Chile trench approx. $993km$ as well as in the depth of about $587km$ and the distance from the Peru/Chile trench approx. $1015km$ the extensions are observed. Between them the aseismic zones are observed. Similarly as in the previous S2 profile case we can analyze the type of earthquake mechanism (compression

versus extension) and compare with the observed data. Figs 10e-g illustrate the normal and tangential components of displacement and stress vectors at the contact boundaries on the descending part of the oceanic lithosphere and also on the bottom of the South American lithosphere for the case of contact stresses. We can indicate five places on the descending lithosphere in the subduction zone and two on the contact boundary with the asthenosphere, where $DUn \neq 0$, but which absolute values over the investigated time interval are small, approx. 100times smaller than in the Villarica volcano case. These places characterize the partially molten rocks. Presented results characterize the very quick and very deep subduction of the Nazca Plate beneath the South American Plate. The tangential component of displacement vector characterizes the mutual movements in the subduction zone as well as on the contact boundary between the lithosphere and the asthenosphere. Figs 10f,g illustrate normal and tangential contact stresses. Their analyses indicate greater values of normal contact stresses with great peaks at the points with coordinates $(268km, 140km)$, $(440km, 108km)$ and $(768km, 100km)$ and with the maximal value of pressure approx. $-6.10^9 Pa$ during the investigated time period, which corresponds to the value of the rate of pressure $\sim -0.06 MPa/yr$ and the contact point with coordinates $(980km, 612km)$ lying in the lower part of the subducted oceanic lithosphere and with the value of pressure of about $-2.045 \times 10^{10} Pa$, which corresponds to the rate of pressure $\sim -0.2045 MPa/yr$ in the end of the subducted oceanic lithospere. Smaller values of normal displacement component have connection with very deep subduction of the Nazca Plate beneath the South American Plate. On the opposite side the normal contact stresses are of one order greater than in the Villarica volcano case. It is really too interesting that the vicinity of contact boundary of the sinking Nazca Plate and the bottom of the South American Plate are partially melted. We see that our numerical results are in a good agreement with observed data.

Analyses of seismotectonics in the Himalayas

In this study we will assume that during a short geological period the invasing Indian plate moves by an uniform velocity $5-6cm/yr$ and that all physical quantities do not depend on the x_2-coordinate. Since time periods between two neighbouring shifts of colliding geological blocks are small, the geological blocks behave elastically.

Nedoma (1998a,b) has discussed the evolution of the Himalayas using the mathematical modelling approach. The model is based on the plate tectonic hypothesis, the theory of multibody contact problems and the finite element metod (Nedoma (1986), (1987), (1990a-c), (1998a)) and taking into account the previous results (e.g. Powell and Conagham (1973); Molnar and Tapponnier (1975), (1978); Klootwijk and Radhakrishnamurty (1981); Nedoma (1986), (1990a,b); Ni (1989); Verma (1991b) and, namely the results of the INDEPTH project (Zhao et al. (1993); Nelson et al. (1996); Makowsky et al. (1996); Brown et al. (1996)). The model shows that the present state of the Himalayas, the Tibet and the Andaman-Nicobar Islands-Sumatra Arc system are a result of geodynamic processes during the previous $140 mil.yrs$. Since the present Indian plate is in collision with the Eurasian plate and subducts beneath the Burmese plate, then the continent-continent model of the Himalayas and the model of subduction of the Indian plate beneath the Burmese plate represent compact geodynamic system. Both mentioned systems are the results of the continuous evolution of these regions during the last $140Ma$, although from the geological point of view its parts are represented by two different geological systems. It is evident that the mathematical simulation of the evolution of the Indian region must be described by the same type of model, as the collision model of the Himalayas and the model of subduction of the Indian plate beneath the Burmese plate, both following from the geodynamical model of evolution of the previous stage, are described by the same mathematical model, where the geometry and the physical parameters are changed in time only.

During the subduction stage the island arc system and several deep faults were developed. The first of these represents the Main Central Thrust (MCT), which in the subduction period of evolution is the main deep fault of the back-thrust belt (in the sense of the Alpine Eocene/Oligicene Alpine orogen of Doglioni et al. (1999)) and which during the next period of the evolution process, characterized by the collision of the Indian plate with the Eurasian plate, changed its position from the initial obligue direction crossing the island arc/back-thrust belt to the present oblique direction with an angle of $30 - 45^o$. The second one was the deep fault situated north from the above area, which during the collision stage was deformed and at present it corresponds to the Indus-Tsampo Suture (ITS) (in

Verma (1991b) denoted as Indus Suture Line). After the collision stage the island arc system was uplifted upto present $5000m$ of hight and at present time it represents the Tibetan Plateau. During the collision stage two main systems of deep faults also originated. Both are situated northward of the Indus-Tsangpo Suture and the first one, we denote it as the Indus-Tsangpo Thrust/Zone (ITZ) (Fig.6a), represents the active thrust of the Landakh Range (see Fig.13.10 of Verma (1991b)), the second one originated northward in the Tibetan Plateau. As the consequence of the continuation shift of the invasion Indian plate the rock formations are folded. The rocks between the MBT and the MCT as well as between the MCT and the ITZ are deformed, which reflect the uplift of the Lesser and High Himalayas. It is envisaged that due to a small angle between the MBT and the MCT, the uplift in the Lesser Himalayas is less in comparison with uplifts in the High Himalayas. The presented geodynamical model allows to clear up also the uplifts and subsidences of geological blocks forming the Himalayan mountains. The mechanism of these uplifts as well as of these subsidences is based on the idea of mutual movements of colliding geological blocks along their common contact boundaries (Fig.1c). Moreover, it allows to clear up also the fact that the sedimentary rocks in the High Himalayas in a great number of cases (like the Mt Everest, etc.) are not folded, but on the contrary they are located in horizontal layers (Nedoma (1998a)).

The investigated area comprises (i) the Indus-Ganga-Brahmaputra plain, the Siwalik Belt of the Sub-Himalayas, the sedimentary belt of the Lesser Himalayas with subordinate volcanics, the Central Crystalline zone of the High Himalayas and the Tethyan Himalayas and (ii) the Shillong Plateau, the Mikir Hill, the Arkan-Yoma fold belt, the Bengal basin with the Andaman-Nicobar Islands arc system and the Burmese plate in the East. In our study we shall limit ourselves for geological periods less than 1×10^5 years in the Andaman - Nicobar Arc system and $1.2 \times 10^5 yrs$ in the Himalayas.

One part of the investigated region is represented by the Himalayan arc system situated in the north part of the investigated region. The model assumes an Indian lithospheric plate $60km$ thick in the Gangetic foredeep and an Eurasian lithospheric plate $180 - 250km$ thick (see Fig.11a). The present motion of the Indian lithospheric plate is assumed to be $5 - 6cm/yr$. The physical data of the model used do not depend on the x_2-coordinate and are taken from the following ranges: densities between $1300kgm^{-3} - 3550kgm^{-3}$, velocities of P waves between $3400km\,\mathrm{sec}^{-1} - 8800km\,\mathrm{sec}^{-1}$ and S waves between $2050kmsec^{-1} - 5160km\,\mathrm{sec}^{-1}$. The geometrical surface configuration of the lithosphere is derived from the distribution of intermediate and deep earthquakes, geological, geophysical as well as geographysical observations (e.g. distributions of deep faults, topography, location of the lower boundary of the lithosphere (see Fig.11a)). The friction of Coulombian type on the contact boundaries is assumed. To model the relative shifting of colliding plates, namely of the invasing plate, the value of the displacement rate vector on the part of the boundary corresponding to the invasing Indian plate is prescribed.

The geodynamic model of the Himalayas in its cross-section profile passing through the Nanda Devi, is presented in Fig.11b. Figures 12a-c present the rate of horizontal component of displacement vector, the so-called rate of convergence, in the area of the Lesser and the High Himalayas and the rate of vertical component of the displacement vector, the so-called rate of uplift, in the detailed area of this area and the normal and tangential components of displacement on the contact boundary between the invasing Indian plate and the Eurasian plate over the investigated time period. The distribution of the rate of principal stresses as well as horizontal, shear and vertical components of the stress rate tensor in the investigated collision zone and the normal and tangential components of stress vector on the contact boundaries between investigated geological bodies are presented in Figs 13a-f. Fig.12a indicates that the rate of convergence between the India and the southern Tibet is of about $23 - 27mm/yr$, between the MBT and the southern Tibet $19.23mm/yr$, between the High Himalayas and the southern Tibet $8mm/yr$ and the Tibetan Plateau and the North Himalayas (south of the ITZ) is of about $11.5mm/yr$. Molnar (1990) believes that the rate of convergence between India and southern Tibet is between $10 - 25mm/yr$. Molnar and Deng (1984) determined the average rate of convergence, based on the sum of seismic moment release this century, of about $17mm/yr$. Lyon-Caen and Molnar (1985), Armijo et al. (1986) determined the convergence between Tibet and India of ˜$15 - 20mm/yr$ and Chandra (1992) determined the rate of convergence at the Himalayas of $18 \pm 7mm/yr$. Velocity field with respect to the South China was analysed by Holt et al. (1991). They show that at the Himalayan mountain front the calculated velocities are between $25mm/yr$ and

$38mm/yr \pm 10mm/yr$ relative to the region of South China. Jackson and Bilham (1994) propose that a conservative vertical velocity for points near the Himalayan divide relative to the central Tibet is of $7.5 \pm 5.6mm/yr$, although the Tibet data have certain uncertainties. Moreover, they also show that the rate of uplift of the High Himalayas relative to the northern plains of India is $6.2 \pm 10mm/yr$ providing a weak upper constraint on the growth of the investigated range. They compare a long-term slip rate model with the morphology of peaks in the Himalayas. Our numerical calculation indicates the rate of uplift of the High Himalayas relative to the northern plains of India of $11 - 15mm/yr$ and for points near the ITZ relative to the Central Tibet is of about $10 - 13mm/yr$. The uplifts ˜$3mm/yr$ e.g. in the Kathmandu valley presented by Jackson and Bilhan (1994) and Pandey et al. (1995) are correct for the above Kathmandu region but not for the High Himalayas as a whole.

In Fig.12c we can observe the bulged out areas situated on the sinking contact boundary between the Indian and the Eurasian plate and on the contact boundary on the bottom of the Eurasian lithospheric plate with asthenosphere. From the thermodynamics it is known that the temperature of melting depends on the pressure. From the numerical computations, based on contact conditions (detailed analysis see Nedoma (1998a)), it follows that $\tau_n \to 0$ and then the temperature of melting decreases, and therefore, the rocks are melted or partially melted. These numerical analyses are in a good agreement with molten areas indicated in the INDEPTH project (Nelson et al. (1996); Makovsky et al. (1996)) and give the theoretical bases for their explanations. Since the deformation energy and the effect of friction acting on the common contact boundaries change into heat then the rocks from these areas heated. It is possible that the eclogites and ophiolites have their origin in the collision processes between the plates. Moreover, our numerical results indicate an uplift of about $19.58mm/yr$ in the High Himalayas (Fig.12b), which is also in a good agreement with geological observations. To say anything about the geodynamical processes in the Himalayas the measurements of the height of the Himalayas must be made. It was exactly 150 years ago that between 1847-1849 James Nicolson measured the Mt Everest height. This measurement was made by the vertical triangulation from points at a distance of more than $150km$, but without taking into account the deflection of verticals produced by the Himalayas and practically without an estimation of the atmospheric reflection. The height was determined as $8840m$. The next measurements were made in 1904, 1954, 1975, 1988, 1992 and 1999. The measurement from 1954 indicates the height $8848m$. Using the Leica photogrammetry equipment in 1988 the National Geographical map of the Mt.Everest region was made, where the Mt. Everest height of $8848m$ was determined. To verify the height of Mt.Everest by using the GPS technique, the climbing expeditions organized by the Chinese National Burreau and Surveying and Mapping (NBSM) and by the Italian National Research Council (CNR) from the Tibetan and the Nepali sides were carried out for September 1992. Instead of the GPS 200 system the measurements were arranged with the distance meters (Leica ME5000, Leica DI3000) and the theodolites (Leica T3000). The measurements were made from several points situated on the Khumbu valley in the Nepal (two GPS 200) and the Rongbuk glacier in the Tibet (two GPS 200) and at the top of Mt.Everest (one GPS 200). Results obtained for Mt. Everest from GPS and terrestrial data (Poretti (1999)) and similar measurements for K2 in 1996 read:

	Mt Everest	K2
Ellipsoidal height at snow level	$8823.51m$	$8591.258m$
Ellipsoid-Geoid separation	$25.14m$	$25.23m$
Depth of snow	$-2.55m$	$-2.22m$
Resulting Geoidal Height	$8846.10 \pm 0.35m$ *a.s.l.*	$8614.27 \pm 0.6m$ *a.s.l.*

The measurement by using the GPS system was also made in 1999 with the measured Mt Everest hight of $8850m$. Analysis of these data indicates the uplift between 1849-1954 yrs, the subsidence between 1954-1992 yrs and the uplift between 1992-1999 yrs. Since the meassured errors are very high due to the unknow snow level and the discrepancy between the geoid and ellipsoid (the unknown deflection of verticals) in 1849 yr, then as a relatively acceptable value can be taken the value less than $2cm/yr$. Subsidences and uplifts can be cleared up by the presented theory, which for a better understanding is presented in the graphical form in Fig.1c. From these analyses we see that our numerical experiments are in a good agreement with the above measurements and analyses. Resulting subsidences and uplifts are generated by movements (shifts) of geological blocks being in mutual contacts along the common contact boundaries between them and under the acting forces resulting

from the movement of the invasing Indian plate. Moreover, blocks between the MBT and the MCT (the Lesser Himalayas) and blocks between the MCT and the ITZ (the High Himalayas) were broken up to a great number of mutually colliding subblocks. The horizontal movement of the invasing Indian plate (approx. $5 - 6cm/yr$) is decomposed on contact surfaces between two neighbouring colliding subblocks into vectors $\mathbf{a}_i, \mathbf{b}_i$. The resulting vector $\mathbf{v}_i$ of vectors $\mathbf{a}_i, \mathbf{b}_i$ represents a value of uplift (similarly for a subsidence). But the mechanism is much more complicated as inside the lithospheric blocks elevations and in the other places also depressions can be observed. Moreover, geological plates and blocks are also deformed and broken up. By such a mechanism the growth of the Lesser and the High Himalayas can be satisfactorily explained (see Fig.1c). On the Earth's surface horizontal components of displacement vector can move in opposite directions in different ends of individual geological blocks. This problem was analysed in Nedoma (1998a) for the case of the foredeep of West Carpathians and where the resulting horizontal and vertical components of displacement vector were comparing with corresponding measured components of recent movements. This effect generally exists, and therefore, it exists regularly also in the Himalayas. To find such effect in the Himalayas the measurements of horizontal and vertical components of recent movements must be measured and analysed.

Our numerical computations of the normal components of displacement and stress vectors also indicate regions with partially molten rocks in regions where the contact boundaries are bulged out (corresponding to areas where condition of non-penetration $u_n^k - u_n^l \neq 0$). The mechanism is the same as in the case of the Andean region and as in the case of the subduction of Indian plate underneath the Burmese plate. The observed anomalous geothermal field in the Himalayas and in the Tibetan region are in an agreement with our numerical results as they are situated in areas where our numerical results indicate the bulged out areas on the main contact boundaries. The observation of the molten rocks is discussed and analysed in Kind et al. (1996); Nelson et al. (1996); Makovsky et al. (1996). From the obtained principal stresses we can indicate where the earthquakes originate and what kind of them can originate in these places. Analysing the rate of principal stresses (see Fig.13a) and the follow-up rates of horizontal, vertical and shear interplate stresses as well as the rate of stress equivalent (Figs 13b-e), we see that in the depth below $70km$ an aseismic zone (gap) is indicated. Intermediate depth earthquakes exist only along Burmese arc and Andaman arc. Great number of Himalayan earthquakes have depths of $10 - 20km$. Several active areas (see Fig. 6a) with small activity south of the ITZ are located at $75° - 93°E$. This suggests that the fault dips down under a certain angle and therefore the epicenters of earthquakes are situated south of the ITZ. The observed facts indicate that the fault is a deep-seated fault and much younger than the ITS. Fig.13f illustrates the normal and tangential stress components on the contact boundary between the Indian plate and the Eurasian plate (i.e between the nodes 98 and 17, we denote it as AB) and between the Eurasian plate and the asthenosphere (i.e. between the nodes 17 and 14, we denote it as BC), and furthermore on the bottom of the invazing Indian plate (i.e. between the contact points 17 and 29, see Fig.13g). From this figure we also observe the maximal pressure at the depth of about $70km$ and at the depth greater than $220km$ and between them the aseismic zone is observed. Numerical calculations (Fig.13a) also indicate the maximal rate of stress build-up ˜$0.02745MPa/yr$ in the depth of about $70km$ below the Himalayas and ˜$0.00263MPa/yr$ near the surface in the Himalayas (Fig.13e).

Analyses of seismotectonic features of the WBZ in the Andaman region

The Andaman-Nicobar islands arc system is situated in the north-eastern Indian Ocean. This island arc system is $1700km$ long and together with the Burmese arc is ˜$2200km$ long and has been formed by sedimentary rocks of very young age. Its origin is related to the subduction of the Indian plate below the Burmese plate. The active subduction is documented by the Barren-Narcondam volcanism (the last eruption of the Barren volcano was in June 1991), by the Wadati-Benioff zone with earthquakes with focal depths up to $200km$, and by anomalous geothermal and gravity fields (Verma (1991b), Das Gupta and Mukhopadhyay (1993)).

The geodynamic model in the cross-section along a regional traverse extending from the Bengal Fan across the North Andaman Island and the Barren-Narcondam volcanic arc system to the Burmese plate is presented at Fig.14 (see Nedoma (1998a,b)). The available geological and seismic data of this region are based on the results of Verma and Mukhopadhyay (1977), Curray et al. (1979), Eguchi,

Uyeda and Maki (1979), Verma (1991b), Das Gupta and Mukhopadhyay (1993) and Nedoma (1998a). The thickness of the Indian subducting plate is assumed to be of about $80km$ while the Burmese plate is assumed to be $85km$ thick. The Indian plate has subducted below the Burmese plate to a depth of about $160km$ in the studied region, of about $180km$ in the region of the Nicobar island arc system and of about $200km$ in the Summatra region. The dip of the Wadati-Benioff zone is of about $40°$ in the studied region and changes to $40° - 50°$ in the Nicobar island and the Summatra regions (Verma and Mukhopadhyay (1977)).

The geodynamic model of the North Andaman Island was constructed on the basis of results of Verma (1991b), DasGupta and Mukhopadhyay (1993) and Nedoma (1990a), (1998a,b). The profile of the model after Verma (1991b) and Das Gupta and Mukhopadhyay (1993) has been slightly modified, since the Andaman Island arc system was originated as a result of the direct motion as well as of the rotation of the Indian plate. Since we simulate the geodynamic processes in the investigated region, we must take into consideration the main direction of the motion of the Indian plate from the rift zone and its rotation, which was the main reason for the modification of the investigated profile. The model used is based on the same ideas as the previous one (see also Nedoma (1998a)) as both models are the profile-models of one great region created by the Indian lithospheric plate, the Eurasian and the Burmese plates. The physical parameters are the following: densities between $2500kgm^{-3} - 3400kgm^{-3}$, velocities of P waves between $3900km\,\mathrm{sec}^{-1} - 7900km\,\mathrm{sec}^{-1}$ and S waves between $2140km\,\mathrm{sec}^{-1} - 4560km\,\mathrm{sec}^{-1}$.

The main results are illustrated in Figures 15a,b and 16a-g. In Fig.15a,b the rate of horizontal component of the displacement vector in the area of the Andaman Island arc and the normal and tangential components of displacement vector are presented. Analysing Fig.15a we see that the rate of convergence between the Indian plate at the place of the Bengal Basin and the Burmese plate is of about ˜$26.9mm/yr$. In Fig.16c-f the rates of horizontal, vertical and shear components of the stress tensor and the rate of stress equivalent are presented, while in Figs 16a,b the rate of principal stresses in the investigated region and in its zoom are illustrated. In Fig.16g the normal and tangential components of stress vector on the contact boundary between the invasing Indian plate and the Burmese plate are given. Numerical results of the normal component of displacement vector and the rate of principal stresses indicate the bulged out regions (connected with the condition of non-penetration on the contact boundaries), where the materials are quickly melted, as from thermodynamics it is known that the temperature of melting depends on the pressure. The mechanism of melting is the same as in previous cases. If the pressure increases the temperature of melting also increases and if the pressure decreases then the temperature of melting also decreases. In Fig.15b we observe anomalous areas with non-penetration condition $DUn \equiv u_n^k - u_n^l \neq 0$, where rocks are melted or partially melted, and therefore, represent anomalous geothermal regions. These regions are built by the Barren-Narcondam volcanic arc and eastward of the Barren-Narcondam volcanic arc by the Alcock Seamont and the eastward anomalous thermal region, which Das Gupta and Mukhopadhyay (1993) consider as the "back-arc rift". These regions indicate the volcano chambers (corresponding to the "black" areas in Fig.16a), namely of the Barren-Narcondam active volcanic arc system. The third anomalous geothermal field is indicated in the Bay of Bengal as on the bottom the oceanic lithosphere bulged out (which follows from the non-penetration condition $DUn \equiv u_n^k - u_n^l \neq 0$), and thus the thickness of the lithosphere is thinner.

Analysing the stress field from Figs 16a-g we find an intermediate seismic gap between $90 - 110km$ depth of the Benioff-Wadati zone. This aseismic zone can be also identified from the rates of horizontal, vertical and shear contact stresses (Figs 16c-e) as well as from the distribution of principal stresses (see Fig.16a and its zoom in Fig.16b). Then from the zoom of principal stresses we can indicate what kind of earthquakes will originate, as we can observe areas of compressions ($\rightarrow\leftarrow$) and areas of extensions ($\leftarrow\rightarrow$). Places of great compressions are indicated below the Andaman island arc system at a depth of approx. $25km$ and eastward in the area of anomalous thermal field (see Nedoma (1998a)) at a depth of about $150 - 160km$ in the subducted lithosphere. On the level of the boundary between the Burmese lithosphere and the asthenosphere at places characterized by the bulged out areas extensions are identified (see the zoom in Fig.16b). The anomalous values Tn correspond to areas with greater pressures (i.e. between the contact points 18 and 29 and at the end of the subducted invasing oceanic lithosphere), the minimal values of Tn correspond to a gap (i.e. between contact points 331 and

35 on the downward part of the oceanic lithosphere). The extensions in the area on the bottom of the Burmese lithosphere and in the asthenosphere right from the subducted lithosphere correspond to the bulged out area and then to the partially melted or melted area. These areas with great pressures and/or great extension (see the zoom in Fig.16b) are the areas of the origin of great earthquakes and of great seismic activity.

3 Conclusion

In the contribution the North part of the Indian Ocean region, occupying the Himalayan collision zone and the Andaman-Nicobar-Sumatra Arc Island system and the Andean subduction zone are analyzed and discussed. The contribution represents continuation of previous results published in Nedoma (1998a,b), Nedoma (1999), Berrocal et al. (2000). It is shown that some present results of plate tectonics can be used for better understanding of evolution processes in the North part of the Indian Ocean region. It is shown that obtained numerical results are in a good agreement with observed geological and geophysical data of the Andean, Himalayan and Andaman-Nicobar regions obtained during the time period of last ten years.

Bibliography

[1] Accocella, V., Vezzoli, L., Omarini, R., Matteini, M., Mazzuoli, R. (2007). Kinematic variations across Eastern Cordillera at $24°S$ (Central Andes): Tectonic and magmatic implications. Tectonophysics 20, 81-92.

[2] Aitchison,J.C., Ali, J.R., Davis, A.M. (2007). When and where did India and Asia collide?, Journal of Gephysical Research, vol 112, B05423, doi: 10.1029/2006JB004706.

[3] Alosanati Tosarova, Z. (2007). Towards understanding the lithosperic structure of the Chilean subduction zone ($36°S-42°S$) and its role in the gravity field. Geophysical Journal International, vol 170, Issue 3, 995-1014.

[4] Armijo,R., Tapponnier,P., Mercier,J.L. and Yong-Liu,H. (1986). Quarternary extension in Southern Tibet: Field observations and tectonic implications. J.Geophys.Res. 91,(B 14), 13803-13872.

[5] Arnbruster, J., Seeber , L. and Jacob, K.H. (1978). The northern termination of the Himalayan mountain front. Active tectonics from micro-earthquakes. J.Geophys.Res., 83, 269-282.

[6] Barazangi, M., Isacks, B.L. (1979). Spatial distribution of earthquakes and subduction of the Nazca Plate beneath South America. Geology 4, 686-692.

[7] Berger, A., Jouanne, F., Hassani, R., Mugnier, J.L. (2004). Modelling the spatial distribution of present-day deformation in Nepal: how cylindrical is the Main Himalayan Thrust in Nepal?, Geophysical Journal International, vol. 156, Issue 1, 94-114.

[8] Berrocal, J., Fernandes, C. (1996a). Seismotectonic features of the Wadatti/Benioff zone in the Andean region. In: Special Issue "Andean Tectonics", (manuscript).

[9] Berrocal, J., Fernandes, C. (1996b). Seismotectonic features of the Wadatti-Benioff zone in the Andean region. Third ISAG, St. Malo (France), 17-19/9/1996.

[10] Berrocal, J., Fernandes, C. (2005). Flat subduction beneath the Andean region from seismological evidences. The 6th Intern. Symposium on Andean Geodynamics, ISAG 2005, 107–110, Barcelona.

[11] Berrocal, J., Nedoma, J., Kestřánek, Z. (2000). Numerical modelling of tectonic evolution of the Wadatti-Benioff zone beneath the Andean region. Proc. 16th World IMACS Congress, Lausanne, Switzerland.

[12] Bhattacharya, S.N. (1992). Crustal and upper mantle velocity structure of India from surface wave dispersion. Cur. Sci, 62, 94-100.

[13] Boyd, T., Snoke, A., Sacks, I.S., Rodrigues, Z.A. (1984). High resolution determination of the Benioff zone geometry beneath southern Peru. Bull. Seismol. Soc. Am. 74, 557-566.

[14] Brown, L.D., Zhao, W., Nelson, K.D., Hauck, M., Alsdorf, D., Ross, A., Cogan, M., Clark, M., Liu, X. and Che, J. (1996). Bright spots, structure and magmatism in Southern Tibet from INDEPTH seismic reflection profiling. Science, 274, 1688-1690.

[15] Cahill, T., Isacks, B.L. (1992). Seismicity and shape of the subducted plate. J. Geophys. Res., 97, 17.503-17.529.

[16] Chander, R., Kumar, V., Paul, D.K. and Khattri, K.N. (1986). On the simulation of stresses in the vicinity of the main central thrust in the Garhwal Himalaya. In: Proc. of Int. Symp. on the Neotectonics in South Asia, Dehradun, India, 137-145.

[17] Chandra, U. (1992). Seismotectonics of Himalaya. Curr. Science, 62, 40-71.

[18] Comte, D., Suarez, G. (1994). An inverted double seismic zone in Chile: evidence of phase transformation in the subducted slab. Science, 263, 212-215.

[19] Comte, D., Roecher, S.W., Suarez, G. (1994). Velocity structure in northern Chile: evidence of subducted oceanic crust in the Nazca plate. Geophys. J. Int. 117, 625-639.

[20] Copley, A., McKenzie, D. (2007). Models of crustal flow in the India-Asia collision zone. Geophysical Journal International, 169,2, 683-698.

[21] Crouzet, C., Gautam, P., Schill, E., Appel, E. (2003). Multicomponent magnetization in western Dolpo (Tethyan Himalaya, Nepal): tectonic implications. Tectonophysics 18, 179-196.

[22] Curray,J.R., Moore,D.G., Lawver,L.A., Emmel,F.J., Raitt,R.W., Henry,M. and Kieckhefer, R. (1979). Tectonics of Andaman Sea and Burma. Mem. Am. Assoc. Pet. Geol. 29, 189-198.

[23] DasGupta, S. and Mukhopadhyay, M. (1993). Seismicity and plate deformation below the Andaman Arc, North-eastern Indian Ocean, Tectonophysics, 225, 529-542.

[24] DasGupta, S., Mukhopadhyay, M., Jana, T.K. (2003). The geometry of the Burmese-Andaman subducting lithosphere. Journal of Seismology, vol. 7., no 2, 155-174.

[25] Delouis, B., Cisternas, A., Dorbath, L., Ribera, L., Kausel, E. (1996). The Andean subduction zone between 22 and 25°S (northern Chile): precise geometry and state of stress. Tectonophysics, 259, 81-100.

[26] Doglioni, C., Harabaglia, P., Merlini, S., Mongelli, F., Peccerillo, A., Piromallo, C. (1999). Orogens and slabs vs. their direction of subduction. Earth-Science Reviews 45, 167-208.

[27] Engdahl, E.R., Van der Hilst, R.D., Berrocal, J. (1995). Imaging of subducted lithosphere beneath South America. Geophys. Ress. Lett. 22, 2317-2320.

[28] Engdahl, E.R., Van der Hilst, R.D., Buland, R.P. (1998). Global teleseismic earthquake relocation with improved travel times and procedure for depth determination. Bull. Seism. Soc. Am., 88, 722–743.

[29] Eguchi, T., Uyeda, S. and Maki, T. (1979). Seismotectonics and tectonics history of the Andaman Sea. Tectonics, 37, 35-51.

[30] Gansser, A. (1964). Geology of the Himalayas, Wiley Interscience Publishers, London.

[31] Grange, F., Hatzfeld, D., Cunningham, P., Molnar, P., Roecker, S.W., Suarez, G., Rodriques, A., Ocola, L. (1984). Tectonic implications of the microearthquakes seismicity and fault plane solutions in southern Peru and their implications. J. Geophys. Res. 89, 6139-6152.

[32] Hasegawa, A., Sacks, I.S. (1981). Subduction of the Nazca plate beneath Peru as determined from seismic information. J. Geophys. Res. 4971–4980.

[33] Holt, W.E., Ni, J.F., Wallace, T.C. and Haines, A.J. (1991). The active tectonics of Eastern Himalayan syntaxis and surrounding region. J.Geophys. Res., 96, 14595-14632.

[34] Jackson, M. and Bilham, R. (1994). Constraints on Himalayan deformation infered from vertical velocity fields in Nepal and Tibet. J.Geophys. Res., v.98, 13897-13912.

[35] Kieckhefer, R. (1979). Tectonics of Andaman Sea and Burma. Mem. Am. Assoc. Pet. Geol. 29, 189-198.

[36] Kind,R., Ni,J., Zhao,W., Wu,J., Yuan,X., Zhao,L., Sandool,E., Reese, Ch., Nabelek,J., Hean, T. (1996). Evidence from earthquake data for a partially molten crustal layer in Southern Tibet. Science, vol. 274, 1692-1694.

[37] Klootwijk, CT. (1979). A review of paleomagnetic data from the Indo-Pakistani fragment of Gondwanaland. In: Geodynamics of Pakistan, Farah Abdul and Dejong, K.A. (Eds), Geol. Surv. Pakistan Quetta, 41-80.

[38] Klootwijk, C.T. and Radhakrishnamutry, C. (1981). Phanerozoic paleomagnetism of the Indian plate and the India-Asia Collision. Paleoreconstruction of Continents. Geodynamics Ser.,Vol. 2, Am.Geophys. Union, 93-105.

[39] Lister, G.S., Forster, M.A., Rawling, F.J. (2001). Episodicity during orogenesis. Geol. Soc. London Spec. Publ., 184, 89-113.

[40] López-Escobar, L., Moreno, H., Cembrano, J. (1995). Geochemistry and tectonics of the Chilean Southern Andes basaltic Quarternary volcanism (37-46°S), Revista Geológica de Chile, vol. 22, no 2, 219-234.

[41] Lyon-Caen, H. and Molnar, P. (1985). Gravity anomalies, flexure of the Indian Plate, and the structure, support and evolution of the Himalaya and Ganga basin, Tectonics, 4, 513-538.

[42] Makowsky, Y. et al. (1996). Structural elements of southern Tethyan Himalayan crust from wide-seismic data. Tectonics, 15, 997-1005.

[43] Mitra, S., Priestley, K., Bhattacharya, A.Kr., Gaur, V.K. (2005). Crustal structure and earthquake focal depths beneath northeastern India and southern Tibet. Geophysical Journal International vol. 160, Issue 1, 227-248.

[44] Molnar, P. (1990). A review of the seismicity and rates of active underthrusting and deformation at the Himalaya. J. Himalayan Geology, 1, 131-154.

[45] Molnar, P. and Tapponnier, P. (1975). Cenozoic tectonic of Asia: Effect of continental collision. Science, 189, 419-426.

[46] Molnar, P. and Tapponnier, P. (1978). Active tectonics of Tibet. J. Geopys. Res., 83, 5361-5375.

[47] Molnar, P, Deng, Q. (1984). Faulting associated with large earthquakes and the average rate of deformation in Central and Eastern Asia. J. Geophys. Res. 89, 6203-6227.

[48] Monsalve, G., Sheehan, A., Schulte-Pelkum, V., Rajaure, S., Pandey, M.R., Wu, F. (2006). Seismicity and one-dimensional velocity structure of the Himalayan collision zone: Earthquakes in the crust and upper mantle. Journal Geophysical Research, vol 111, B10301, doi: 10.1029/2005JB004062, 2006.

[49] Mukhopadhyay, M. (1984). Seismotectonics of subduction and back-arc rifting under the Andaman Sea. Tectonophysics, 108, 229-239.

[50] Mukhopadhyay, M. (1992). On earthquake focal mechanism studies for Burmese Arc, Current Science, 62, 72-85.

[51] Mukhopadhyay, M. and Das Gupta S. (1988). Deep structure and tectonics of Burmese arc: Constraints from earthquake and gravity data. Tectonophysics, 149, 299-322.

[52] Nedoma, J. (1986). On the geodynamic model of the Earth and plate tectonic hypothesis, I-III. Gerlands Beitr. Geophysik, 95(1), 36-62, 95(2),89-105.

[53] Nedoma, J. (1987). On the Signorini problem with friction in linear thermo-elasticity: the quasi-coupled 2D case. Appl. Math., 32(3), 186-199.

[54] Nedoma, J. (1990a). Tectonic evolution of collision zones, I-II. Gerlands Beitr.Geophysik, 99 (2),97-108, 109-121.

[55] Nedoma, J. (1990b). Plate tectonics and the analyses of fracture mechanisms in a collision zone, I-II. Contrib. Geophys. Inst. Slov. Acad.Sci., 20, 53-96, 21, 38-58.

[56] Nedoma, J. (1990c). On a new theory of earthquake mechanism. In: Proc.4th Symp. on Analysis of Seismicity and Seismic Risk, In: Z. Schenkova, ed., Geophys. Inst., Czech. Acad. Sci., Prague, 339-346.

[57] Nedoma, J. (1998a). Numerical Modelling in Applied Geodynamics, John Wiley&Sons, Chichester, New York, pp. 966.

[58] Nedoma, J. (1998b). Geodynamic analyses of the Himalayas and the Andaman Islands based on mathematical simulation of geodynamic processes. The 19th General Assembly of the IAESPEI, August 18-28, 1997, Thessaloniki, also in Technical Report No 776, Institute of Computer Science AS CR, Prague.

[59] Negi, J.G., Pandey, O.P., and Agrawal, P.K. (1986). Super-Mobility of Hot Indian Lithosphere, Tectonophysics, 131, 147-156.

[60] Nelson, D. et al. (1996). Partially molten middle crust beneath S. Tibet. Synthesis of Project INDEPTH. Results. Science, 274, 1684-1687.

[61] Ni, J. and Barazangi, M. (1984). Seismotectonics of the Himalayan collision zone: geometry of the underthrusting Indian plate beneath the Himalaya. J. Geopys. Res., 89(B2), 1147-1163.

[62] Ni, J. (1989). Active tectonics of the Himalaya. Proc. Ind.Acad.Sci., 98, 71-89.

[63] Panday, M.R., Tandukar, R.P., Avouac, J.P., Lave, J., and Massot, J.P. (1995). Interseismic Strain Accumulation on the Himalayan Crustal Ramp (Nepal), Geophys. Res. Letters, v.22, 751-754.

[64] Poretti,G. (1999). 150 yrs of measuring the Himalayas. Reporter 41, The Magazine of Leica Geosystems, 13-17.

[65] Powell, C.M. and Conagham, P. (1973). Plate tectonics and the Himalayas. Earth and Planet. Sci. Lett. 20, 1-22.

[66] Quitmeyer, R.C. and Jacob, K.H. (1979). Historical and modern seismicity of Pakistan, Afganistan and South-east Iran. Bull. Seis. Soc. Am., 69, 773-823.

[67] Radha, K.M., Sanu, T.D. (2002). Shallow seismicity, stress distribution and crustal deformation pattern in the Andaman-West Sunda arc and Andaman Sea, northern Indian Ocean. Journal of Seismology, vol. 6., no 1, 25-41.

[68] Ramesh, D.S. (2005). Moho geometry and upper mantle images of northeast India. Geophysical Research Letters, 32:14, L14301.

[69] Ramos, V., Folguera, A. (2005). Tectonic evolution of the Andes of Neuquen: constraints derived from the magmatic arc and foreland deformation. In: Veiga, G.D. et al. (Eds) Geol. Soc. London, Special Publ., 252, 15-35.

[70] Rastogi, B.K. (1974). Earthquake mechanisms and plate tectonics in the Himalayan region. Tectonophysics 21, 47-56.

[71] Rodrigues, L., Tavera, J. (1991). Determinación con alta resolutión dela geometria dela zona Wadati-Benioff en el Peru central. Rev. Bras. Geof.

[72] Sato,K., Bhatia, S.C. and Gupta, H.K, (1996). Three-Dimensional Numerical Modelling of Deformation and Stress in the Himalaya and Tibetan Plateau with a Simple Geometry. J.Phys.Earth. 44, 227-254.

[73] Singh, D.D., Li,Q. and Nyland, E., (1990). Lithospheric deformation beneath the Himalayan region. Phys.Earth Planet.Inter., 61, 291-296.

[74] Solon, K.D., Jones, A.G., Nelson, K.D., Unsworth, M.J., Kidd, W.F., Wei, W., Tan, H., Jin, S., Deng, M., Booker, J.R., Li, S., Bedrosian, P. (2005). Structure of the crust in vicinity of the Banggong-Nujiang suture in Central Tibet from INDEPTH magnetotelluric data. Journal of Geophysical Research, vol. 110, B10102, doi:10.1029/2003JB002405.

[75] Spencer, E.D. (Ed.) (1973). Mesozoic-Cenozoic orogenic belts. Data for orogenic studies. Geol. Soc. London, Scot. Acad. Press, Edinburg, 809pp.

[76] Tassara, A., Götze, H.-J., Schmidt, S., Hackney, R. (2006). Three-dimensional density model of the Nazca plate and the Andean continental margin. Journal of Geophysical Research, vol.111, BO9404, doi:10.1029/2005JB003976.

[77] Tavera, H., Bufon, E. (2001). Source mechanism of earthquakes in Peru. Journal of Seismology, vol.5, no 4, 519-540.

[78] Valdiya, K.S. (1984). Aspects of Tectonics, Tata McGraw Hill Publishers, New Delhi.

[79] Verma,R.K. (1991a). Seismicity of the Himalaya and NE India and the nature of continent-continent collision. Physics and Chemistry of the Earth, v.18, 345-370.

[80] Verma,R.K. (1991b). Geodynamics of the Indian Peninsula and the Indian Plate Margin. Oxford and IBH Publication, N. Delhi.

[81] Verma, R.K., Mukhopadhyay, M. (1977). An analysis of gravity field in North-Eastern India. Tectonophysics, 42, 283-317.

[82] Verma, R.K., Mukhopadhyay, M., Bhuin, N.C. (1978). Seismicity, gravity and tectonics in Andaman Sea. J. Phy. Earth, 26, 233-248.

[83] Verma, R.K. and Kumar, G.V.R.K. (1987). Seismicity and the nature of plate movement along the Himalayan arc, North-East India and Arakan-Yoma: A review, Tectonophysics, 134, 153-175.

[84] Vilotte, J.P., Madariaga, R., Daignieres, M. and Zienkiewicz, O.C. (1986). Numerical study of continental collision: influence of buoyancy forces and a stiff inclusion. Geophys. J. R. Astron. Soc., 84, 279-319.

[85] Wang C.Y., Shi,Y. and Zhou, W.H (1982), On the tectonics of the Himalaya and the Tibet plateau. J.Geophys. Res, 87, 2949-2957.

[86] Week, A., Harisson, R.N., Peter, G. (1967). Island arc system in Andean Sea. Am. Assoc.Pet. Geol. Bull. 51, 1805-1815.

[87] Zhao, W. and Morgan, W.J. (1985). Uplift of Tibetan plateau. Tectonics 4, 359-369.

[88] Zhao, W., Nelson, K.D. and Project INDEPTH Team (1993). Deep seismic reflection evidence for continental underthrusting beneath southern Tibet. Nature 336, 557-559.

Acknowledgement

The research was partially supported by the grant COPERNICUS-HIPERGEOS II - KIT No. 977006.

Figures

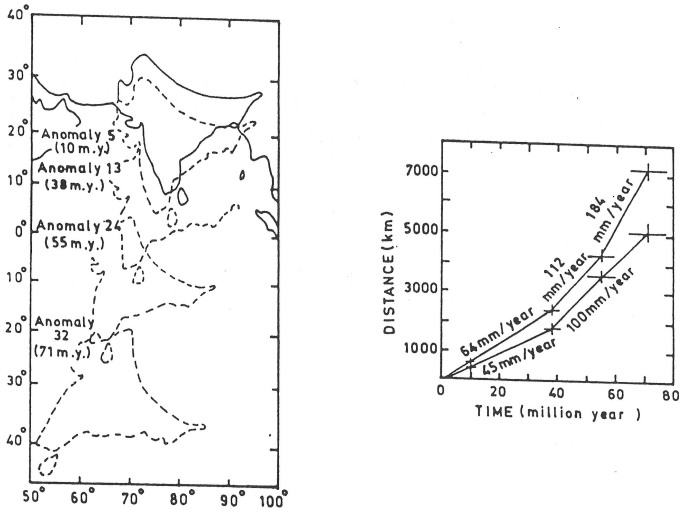
40°
30°
20°
10°
0°
10°
20°
30°
40°
50°
60°
70°
80°
90°
100°
Anomaly 5
(10 m.y.)
Anomaly 13
(38 m.y.)
Anomaly 24
(55 m.y.)
Anomaly
32
(71 m.y.)
DISTANCE (km)
7000
5000
3000
1000
0
20
40
60
80
TIME (million year)
64mm/year
112
mm/year
184
mm/year
45mm/year
100mm/year

(a)

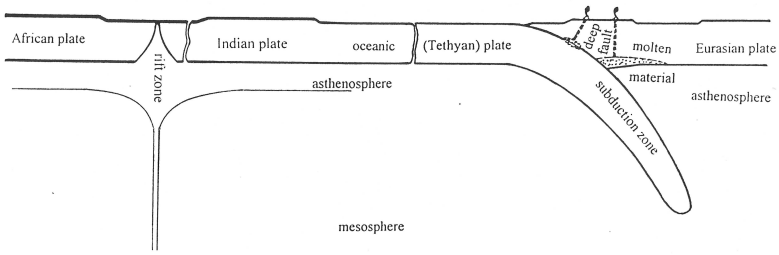
African plate
rift zone
Indian plate
oceanic
asthenosphere
mesosphere
(Tethyan) plate
deep
fault
molten
material
Eurasian plate
asthenosphere
subduction zone

(b)

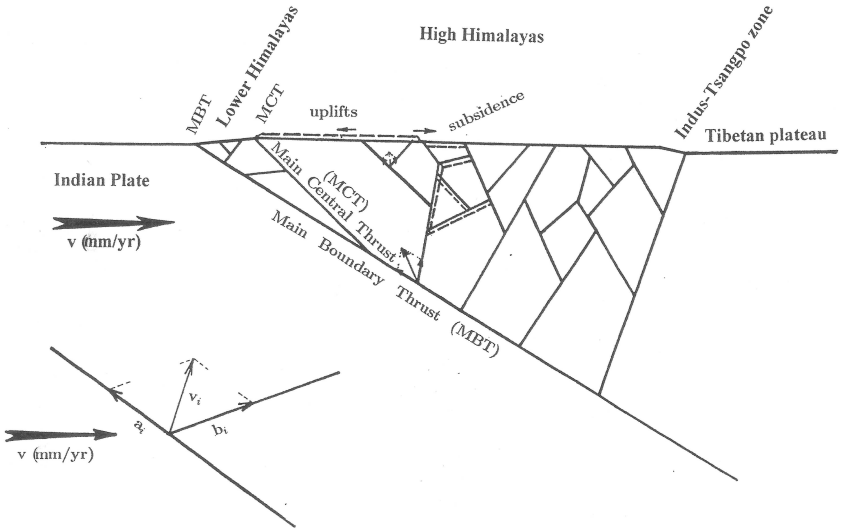

(c)

Fig. 1. Evolution process of collision between the India and the Eurasian plate.
(a) Position of India with respect to the rest of Eurasia at different times in the past and the distance as a function of time for the NE and NW tips of India with respect to their present position (after Molnar and Tapponnier (1975); see also Verma (1991b), p.280),
(b) subduction process (after Nedoma (1998a)),
(c) mechanism of uplifts and subsidences.

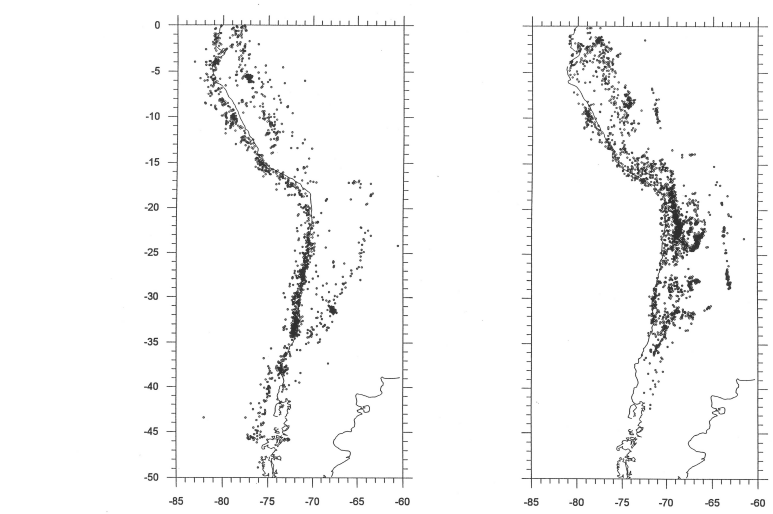

(a) (b)

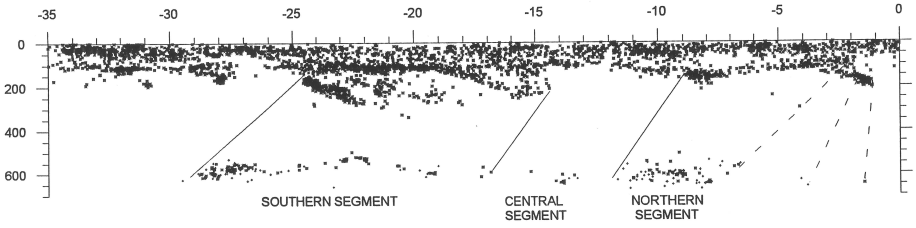

(c)

Figs 2a,b,c. Seismic activity in the Andes occured in the time period 1964-1995 (Berrocal, Fernandes (1996a)).
(a) The epicentres of events with $h \leq 50km$.
(b) The epicentres of events with $h > 50km$.
(c) The longitudinal $S - N$ section of Andean seismicity based on selected hypocentres occured in the time period 1964-1995.

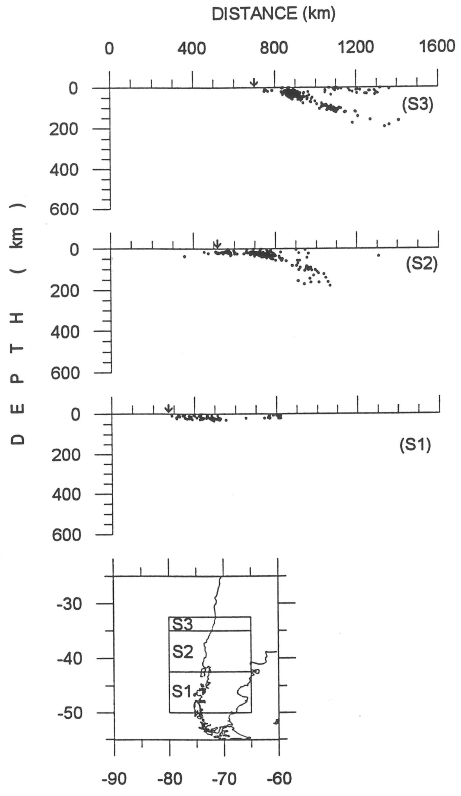
DISTANCE (km)
0
400
800
1200
1600
0
200
400
600
(S3)
(S2)
(S1)
D E P T H (km)
-30
-40
-50
S3
S2
S1
-90
-80
-70
-60

(a)

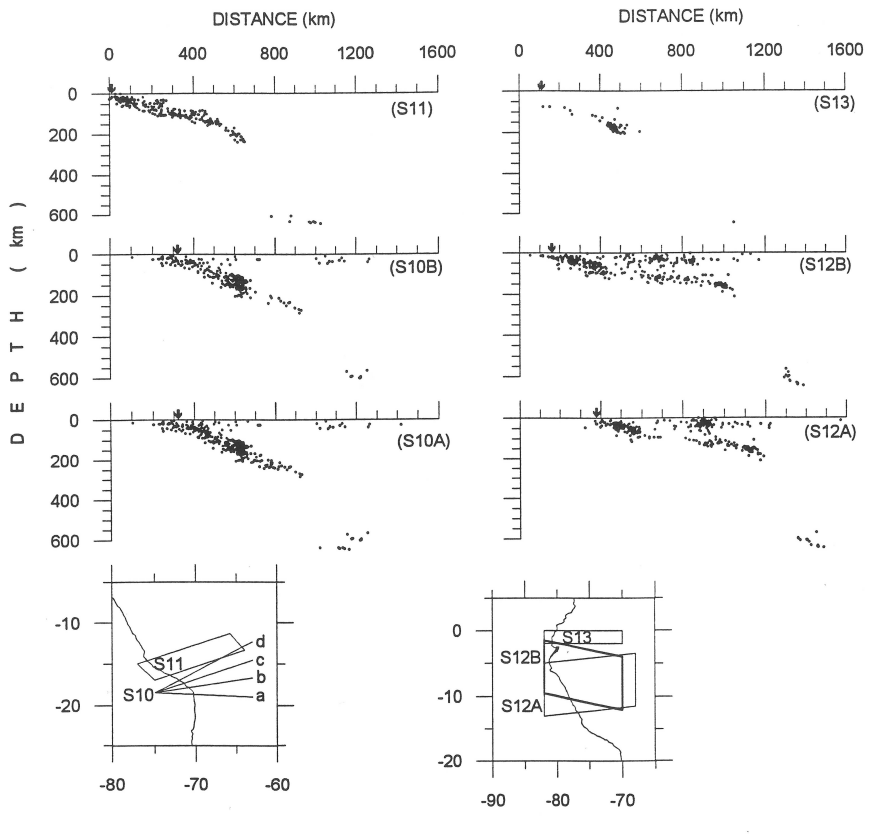

(b)

Figs 3a,b. Seismic activity in the Southern Chile, cross sections projected in vertical planes normal to the Andean region, constructed with activity occured in the time period 1964-1995 (Berrocal, Fernandes (1996a)):
(a) cross section S2 (Southern Chile),
(b) cross section S10B (Chile-Peru border).

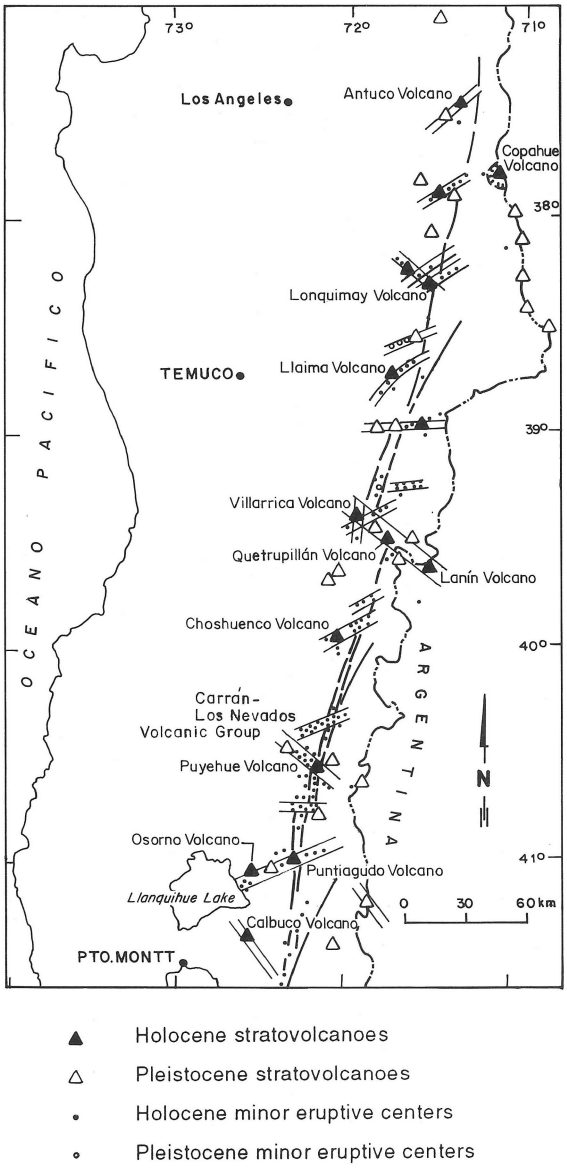

Fig. 4. The Southern volcanic Zone of the Andes (López-Escobar et al. (1995))

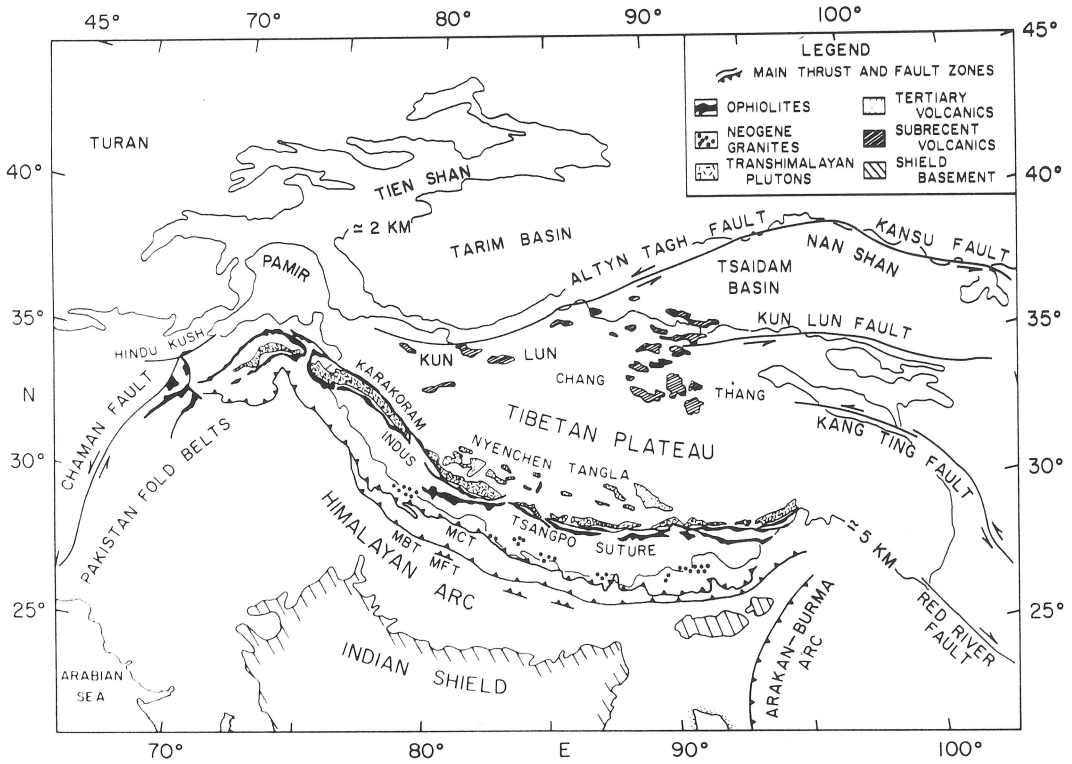

Fig.5a. Geotectonic map of the Himalayas and the adjoining region (modified after Gansser (1964), Molnar, Taponier (1975), see Sato et al. (1996)).

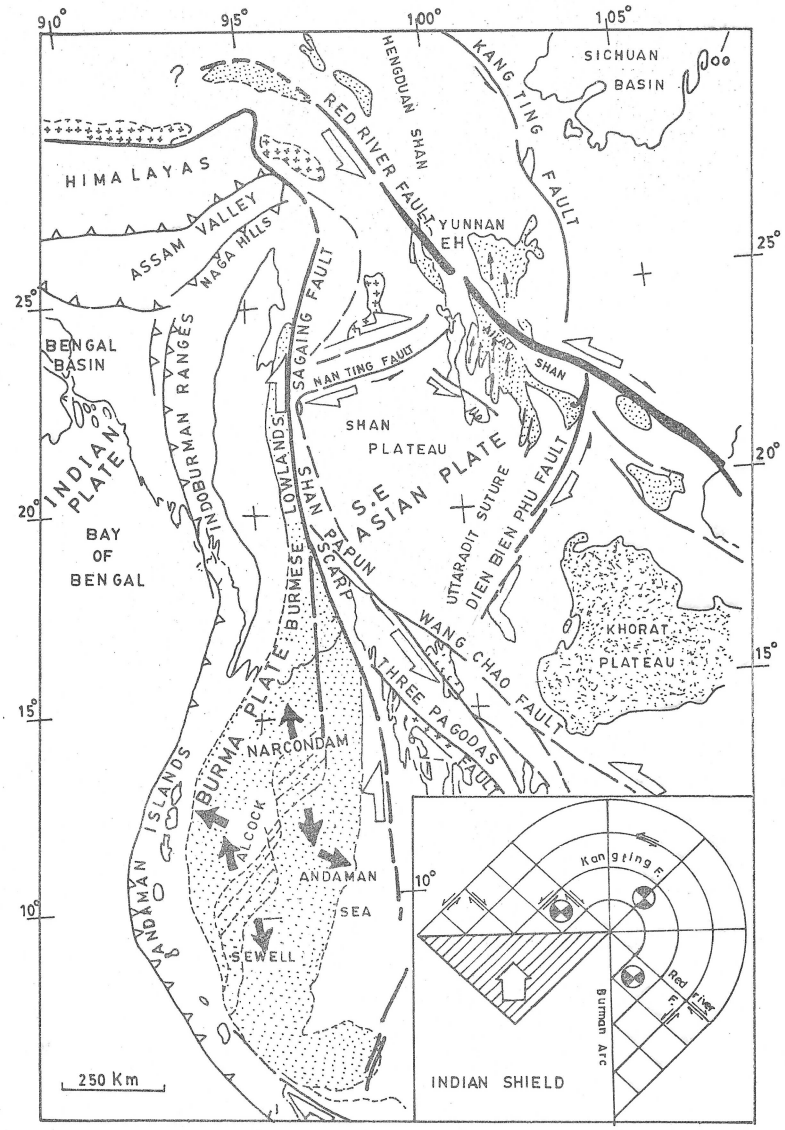

Fig.5b. Major structural elements of the Andaman arc and of the Barmese arc (Mukhopadhyay (1992)).

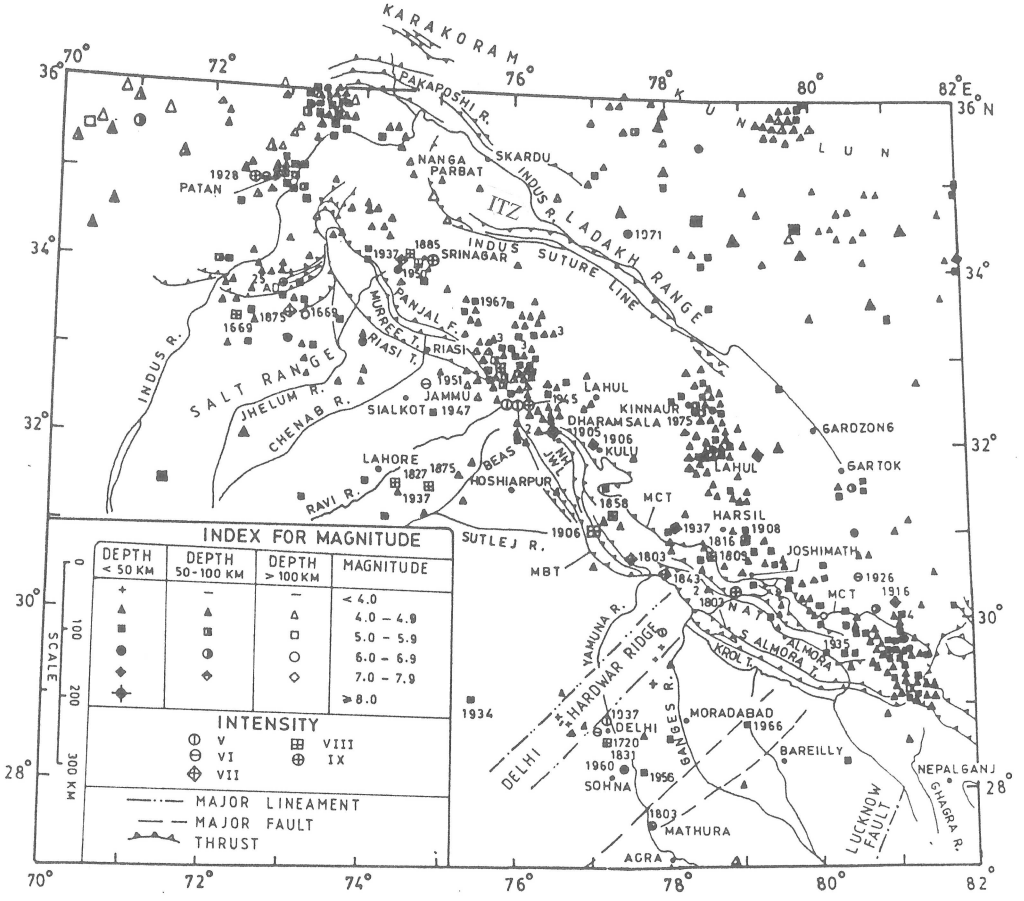

Fig.6a. Seismic activity in the Himalayas (after Verma (1991b)).

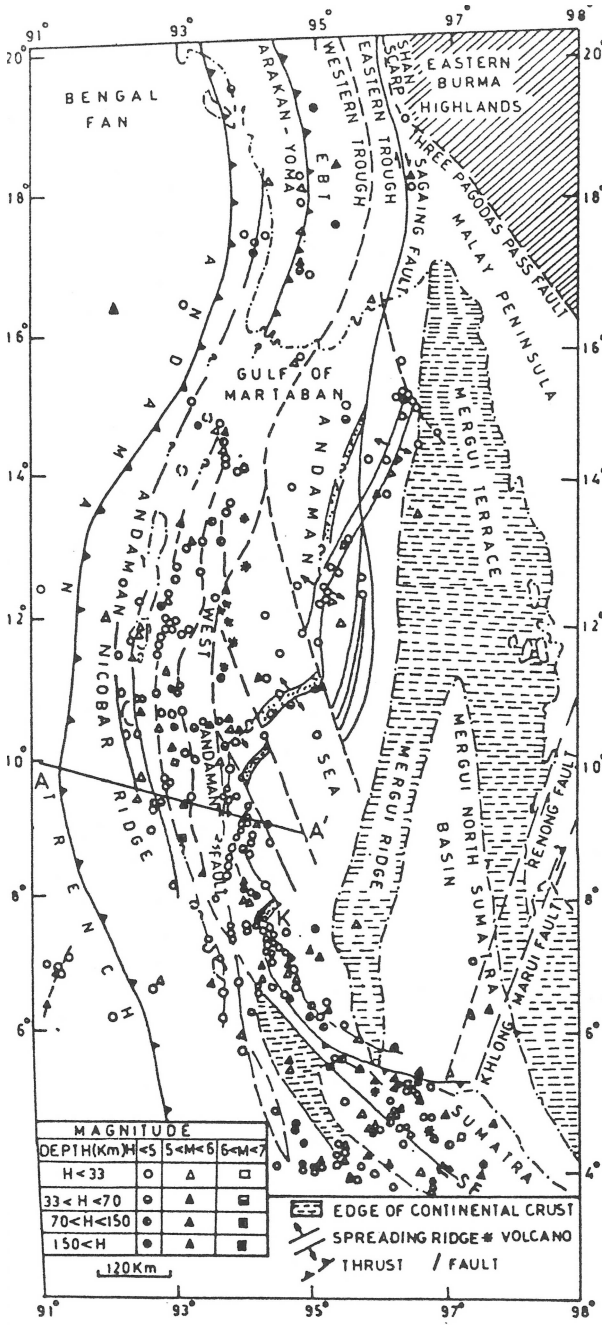

Fig.6b. Seismic activity in the Andaman Sea for the period 1960-1980 (after Curray et al. (1979), Verma (1991b); Mukhopadhyay (1984)).

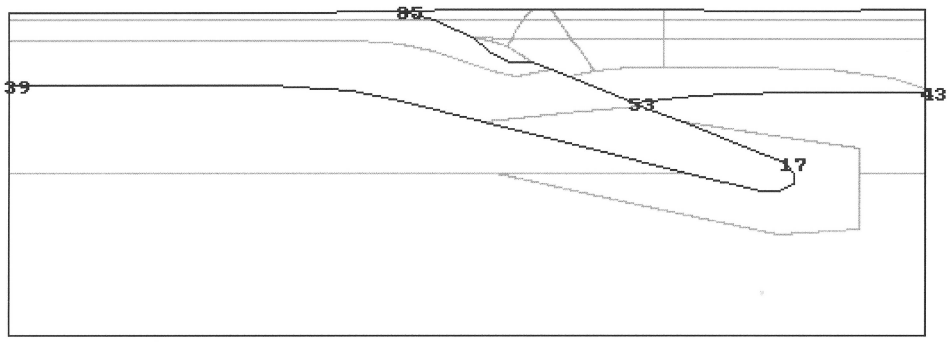

Fig. 7. The profil S2 across the Villarica volcano - the model.

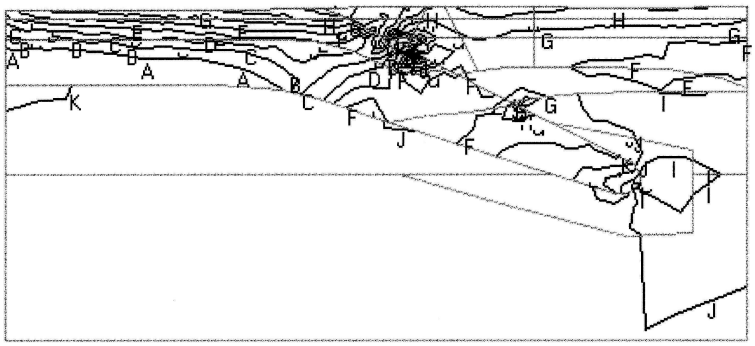

(a)

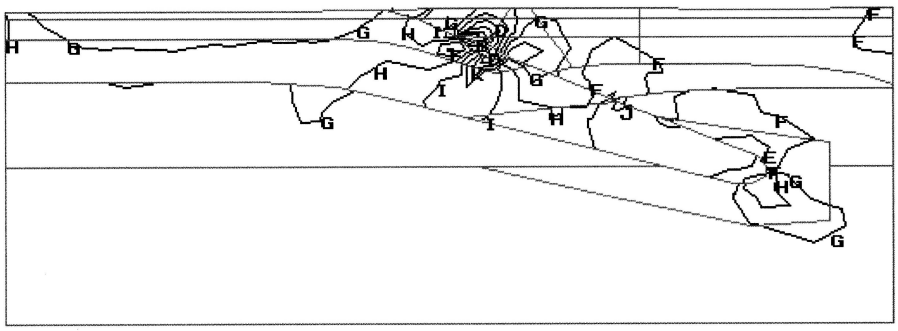

(b)

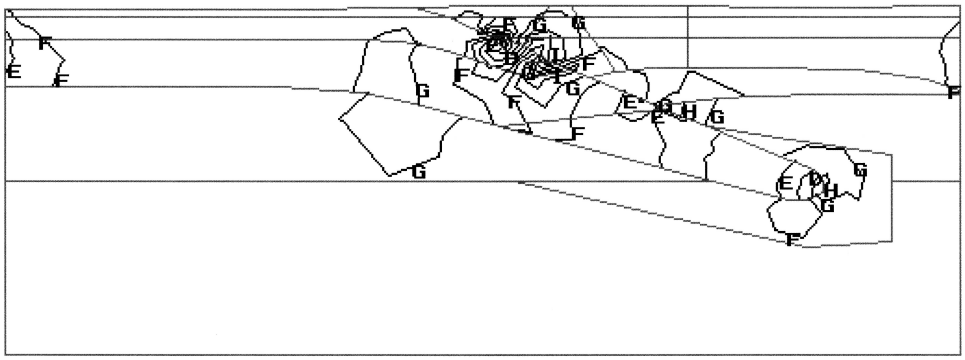

(c)

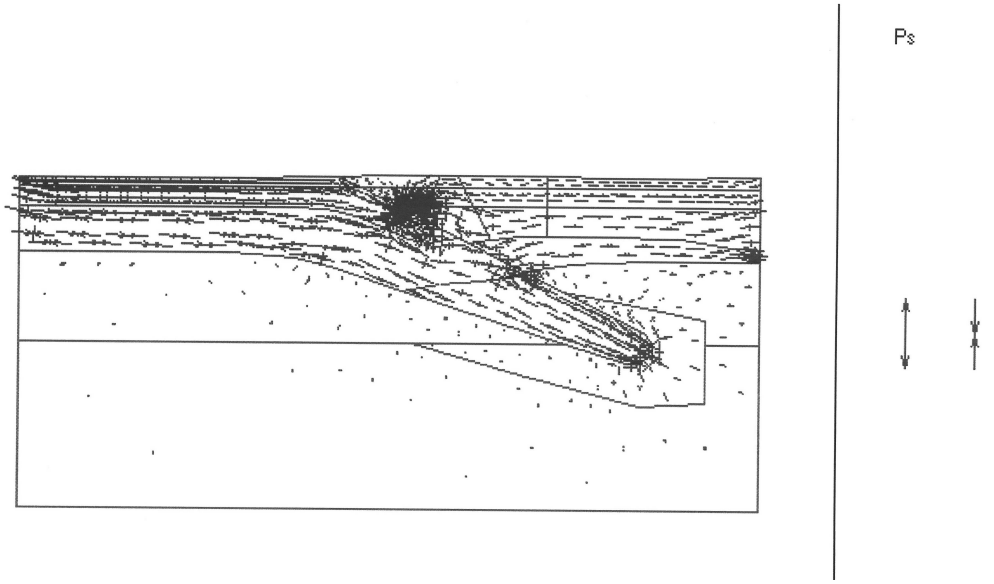

(d)

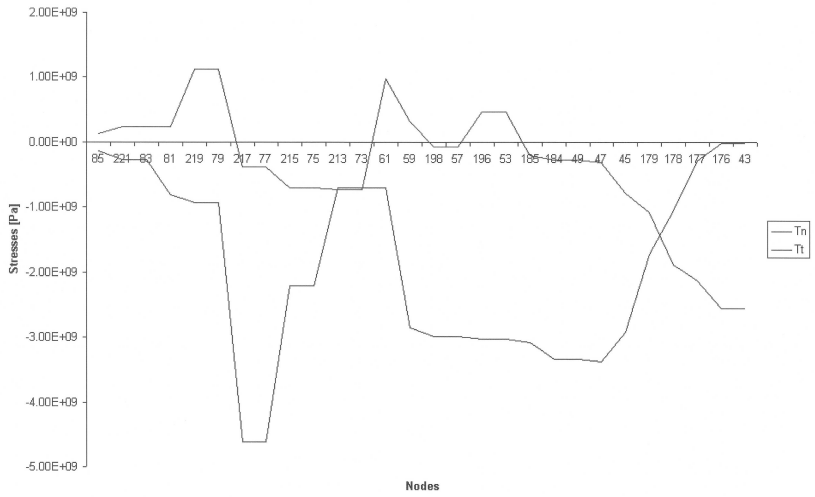
2.00E+09
1.00E+09
0.00E+00
-1.00E+09
-2.00E+09
-3.00E+09
-4.00E+09
-5.00E+09
Stresses [Pa]
85 221 83 81 219 79 217 77 215 75 213 73 61 59 198 57 196 53 185 184 49 47 45 179 178 177 176 43
Nodes
Tn
Tt

(e)

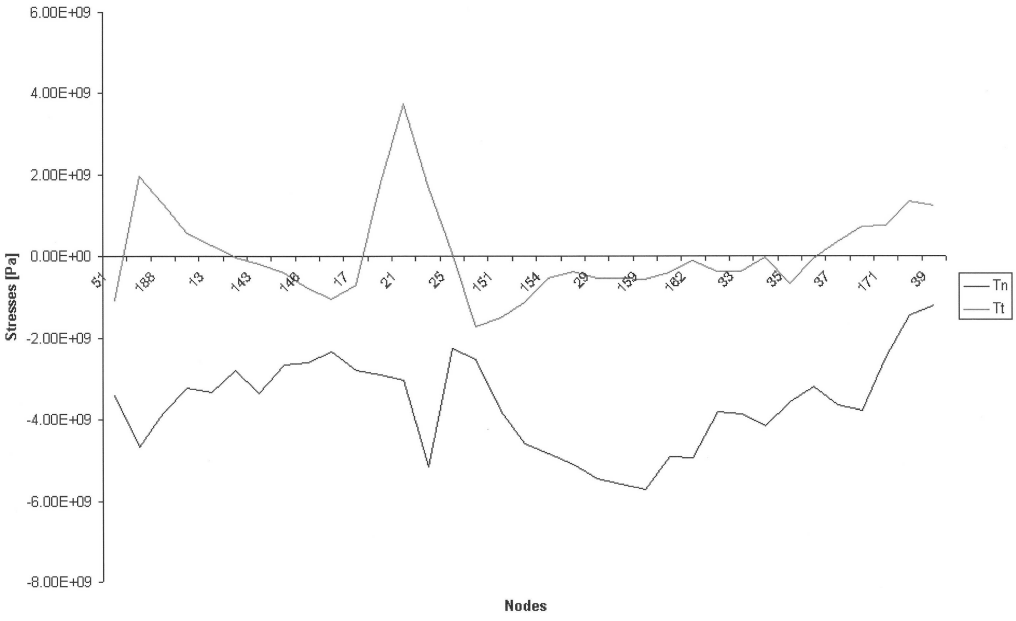
6.00E+09
4.00E+09
2.00E+09
0.00E+00
-2.00E+09
-4.00E+09
-6.00E+09
-8.00E+09
Stresses [Pa]
188 13 143 146 17 21 25 151 154 29 159 162 33 35 37 171 39
Nodes
Tn
Tt

(f)

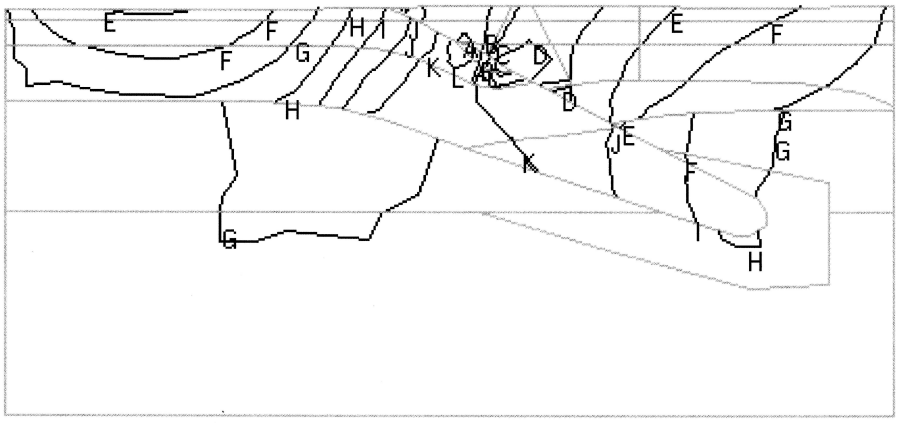
E
F
G
H
I
J
K
L
D
A
B
C

(g)

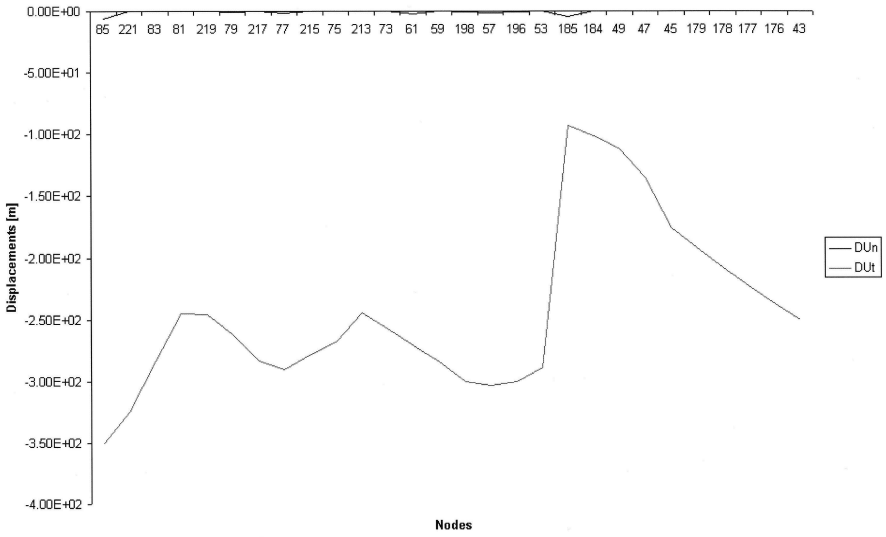
0.00E+00
-5.00E+01
-1.00E+02
-1.50E+02
-2.00E+02
-2.50E+02
-3.00E+02
-3.50E+02
-4.00E+02
Displacements [m]
85 221 83 81 219 79 217 77 215 75 213 73 61 59 198 57 196 53 185 184 49 47 45 179 178 177 176 43
Nodes
DUn
DUt

(h)

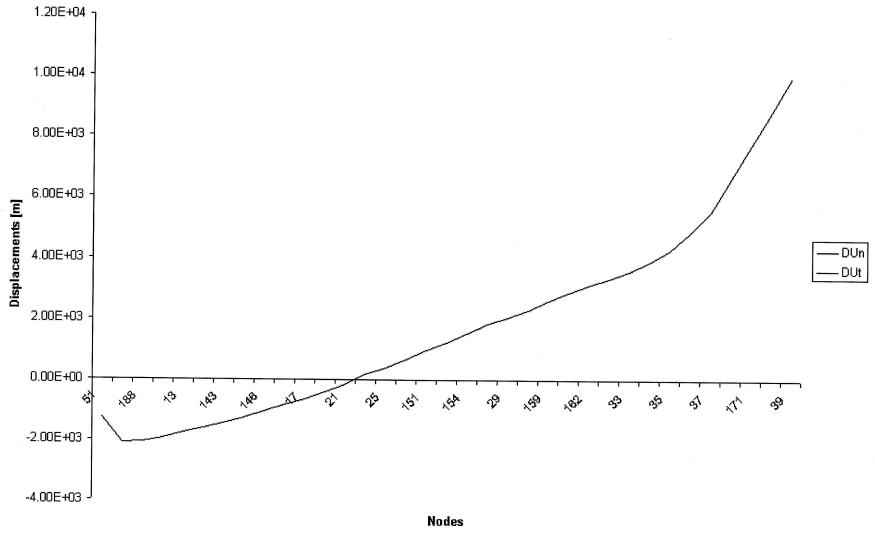

(i)

Figs 8a-i. The profile S2 across the Villarica volcano.
(a) Distribution of the rate of interplate horizontal stress component $(Sx, [MPa/yr])$ $A = -0.0355$, $B = -0.0317$, $C = -0.0278$, $D = -0.024$, $E = -0.0202$, $F = -0.0164$, $G = -0.0125$, $H = -0.0087$, $I = -0.00487$, $J = -0.00104$, $K = 0.002788$, $L = 0.00662$.
(b) Distribution of the rate of the interplate shear stress component $(Sxz[MPa/yr])$ $A = -0.01499$, $B = -0.01223$, $C = -0.00948$, $D = -0.00672$, $E = -0.00396$, $F = -0.001203$, $G = 0.001553$, $H = 0.00431$, $I = 0.007069$, $J = 0.009826$, $K = 0.01258$, $L = 0.01534$.
(c) Distribution of the rate of interplate vertical stress component $(Sz[MPa/yr])$ $A = -0.03138$, $B = -0.02585$, $C = -0.02032$, $D = -0.01479$, $E = -0.009266$, $F = -0.003735$, $G = 0.001795$, $H = 0.007326$, $I = 0.01285$, $J = 0.01838$, $K = 0.02391$, $L = 0.02944$.
(d) Distribution of the rate of intraplate principal stresses (max.$|0.0652|$ $[MPa/yr]$) two times magnified.
(e) The normal and tangential components of stress vector on the contact boundary between points $(85, 53, 43)$.
(f) The normal and tangential components of stress vector on the contact boundary between points $(53, 17, 39)$.
(g) Distribution of the rate of interplate vertical component of displacements $(Uz[mm/yr])$ $A = -1.626$, $B = -1.365$, $C = -1.104$, $D = -0.8433$, $E = -0.5822$, $F = -0.321$, $G = -0.0599$, $H = 0.2012$, $I = 0.4623$, $J = 0.72335$, $K = 0.9846$, $L = 1.245$.
(h) The normal and tangential displacement component over the investigated time period on the contact between points $(85, 53, 43)$.
(i) The normal and tangential displacement component over the investigated time period on the contact between points $(53, 17, 39)$.

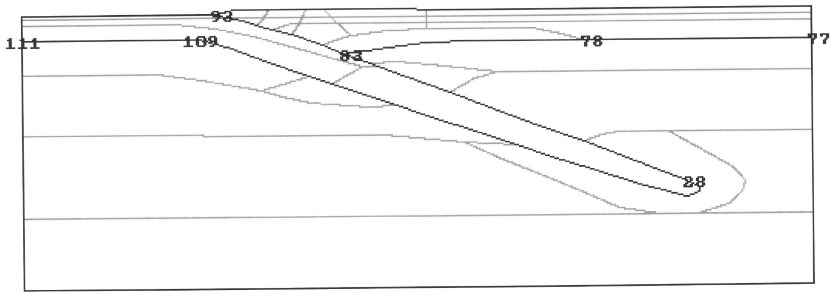

Fig.9. The profile S10B across the Peru-Chile border - the model.

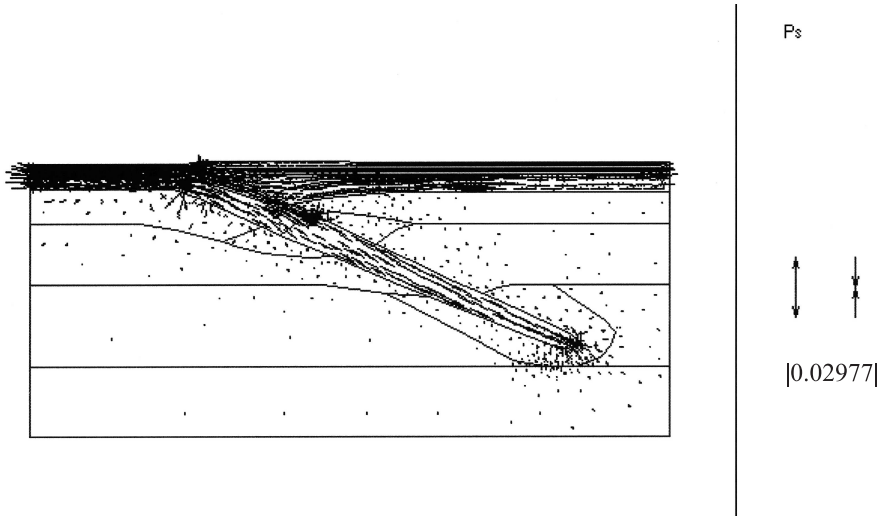

(a)

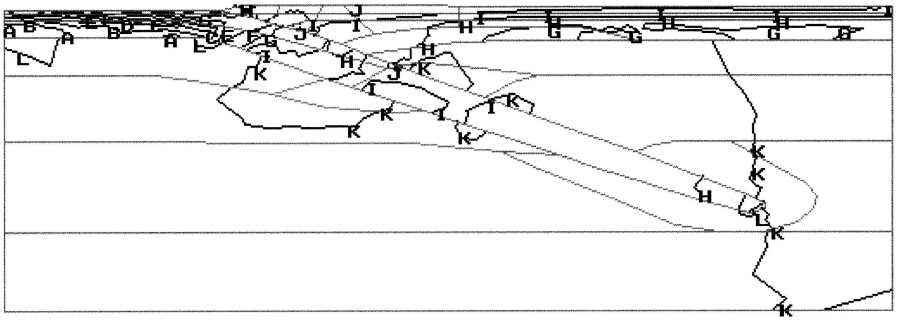

(b)

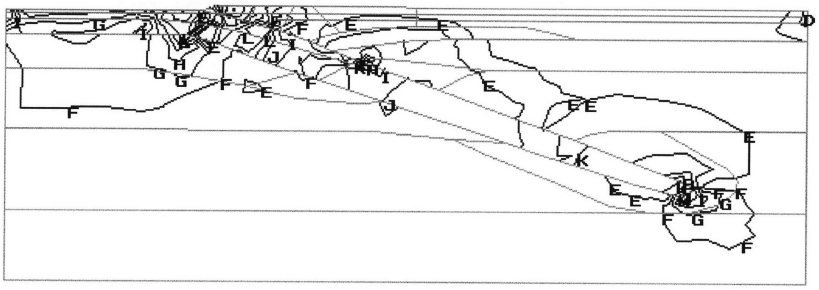

(c)

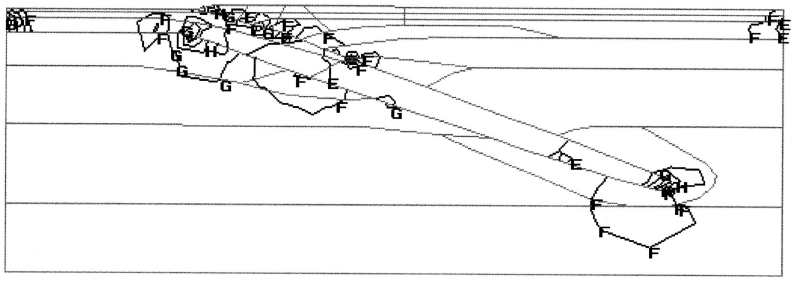

(d)

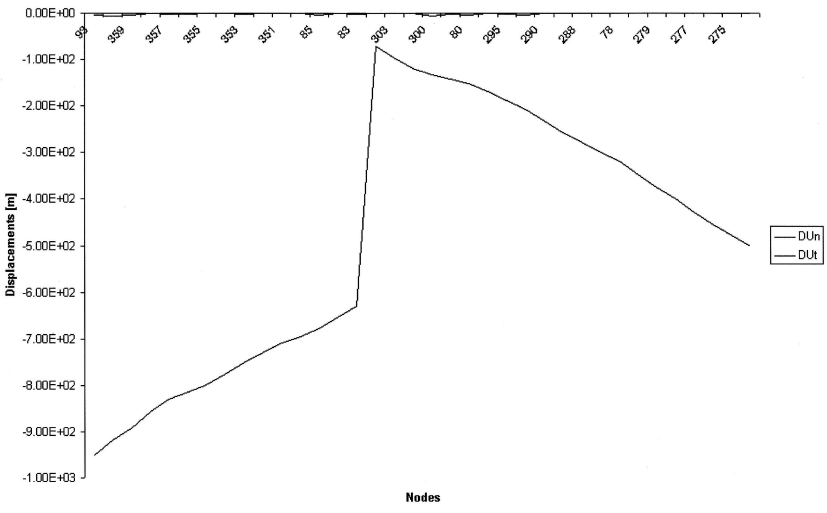
0.00E+00
-1.00E+02
-2.00E+02
-3.00E+02
-4.00E+02
-5.00E+02
-6.00E+02
-7.00E+02
-8.00E+02
-9.00E+02
-1.00E+03
Displacements [m]
99
359
357
355
353
351
85
83
303
300
80
295
290
288
78
279
277
275
Nodes
DUn
DUt

(e)

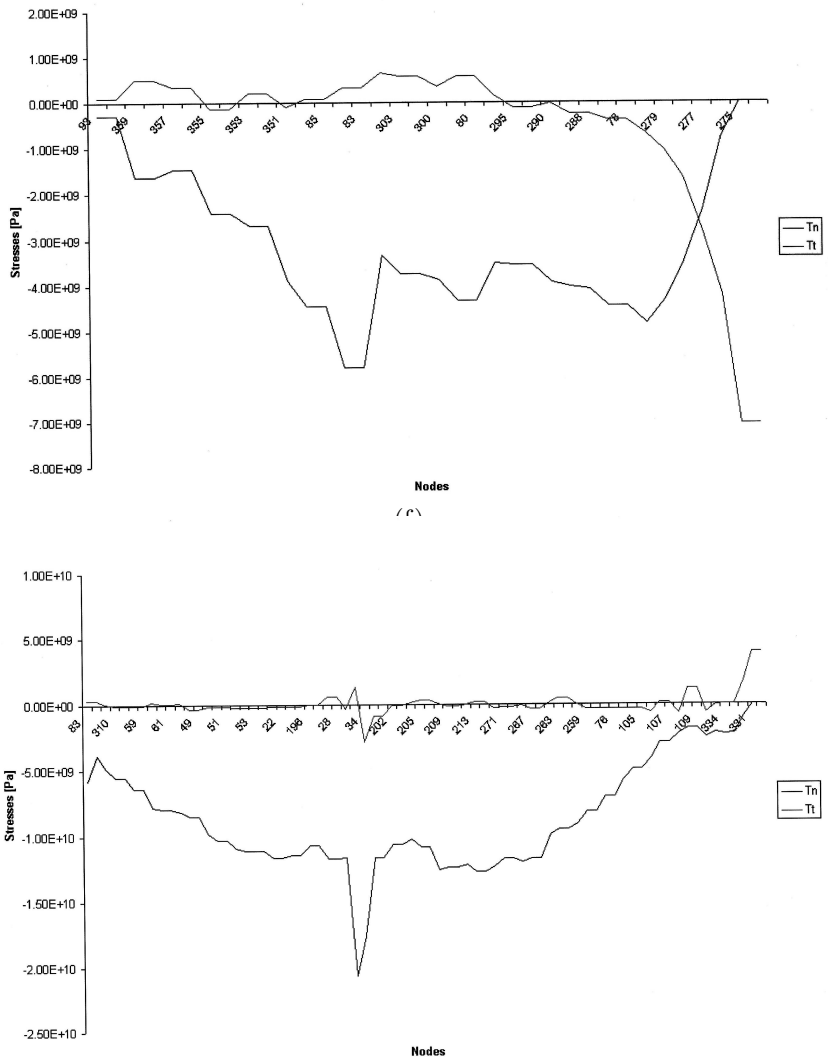

(g)

Figs 10a-g. The profile S10B across the Peru-Chile border:
(a) Distribution of the rate of interplate horizontal stress component $(Sx, [MPa/yr])$ $A = -0.02524$, $B = -0.02274$, $C = -0.02024$, $D = -0.01773$, $E = -0.01523$, $F = -0.01273$, $G = -0.01023$, $H = -0.007728$, $I = -0.005225$, $J = -0.002723$, $K = -0.0002203$, $L = 0.002282$.
(b) Distribution of the rate of the interplate shear stress component $(Sxz[MPa/yr])$ $A = -0.002755$, $B = -0.002129$, $C = -0.001503$, $D = -0.0008767$, $E = -0.0002504$, $F = 0.0003758$, $G = 0.001002$, $H = 0.001628$, $I = 0.002254$, $J = 0.002881$, $K = 0.003507$, $L = 0.004133$.
(c) Distribution of the rate of interplate vertical stress component $(Sz[MPa/yr])$ $A = -0.008852$, $B = -0.007204$, $C = -0.005556$, $D = -0.003909$, $E = -0.002261$, $F = -0.0006138$, $G = 0.001033$, $H = 0.002681$, $I = 0.004329$, $J = 0.005976$, $K = 0.007624$, $L = 0.009272$.
(d) Distribution of the rate of intraplate principal stresses (max. $|0.02977|$ $[MPa/yr]$ two times magnified).
(e) The normal and tangential displacement component DUn, DUt $(\left[m/10^5 yr\right])$ on the contact between points $(93, 83, 77)$.
(f) The normal and tangential of contact stresses Tn, Tt $(\left[Pa/10^5 yr\right])$ on the contact between points $(93, 83, 77)$.
(g) The normal and tangential of contact stresses Tn, Tt $(\left[Pa/10^5 yr\right])$ on the contact between points $(83, 28, 111)$.

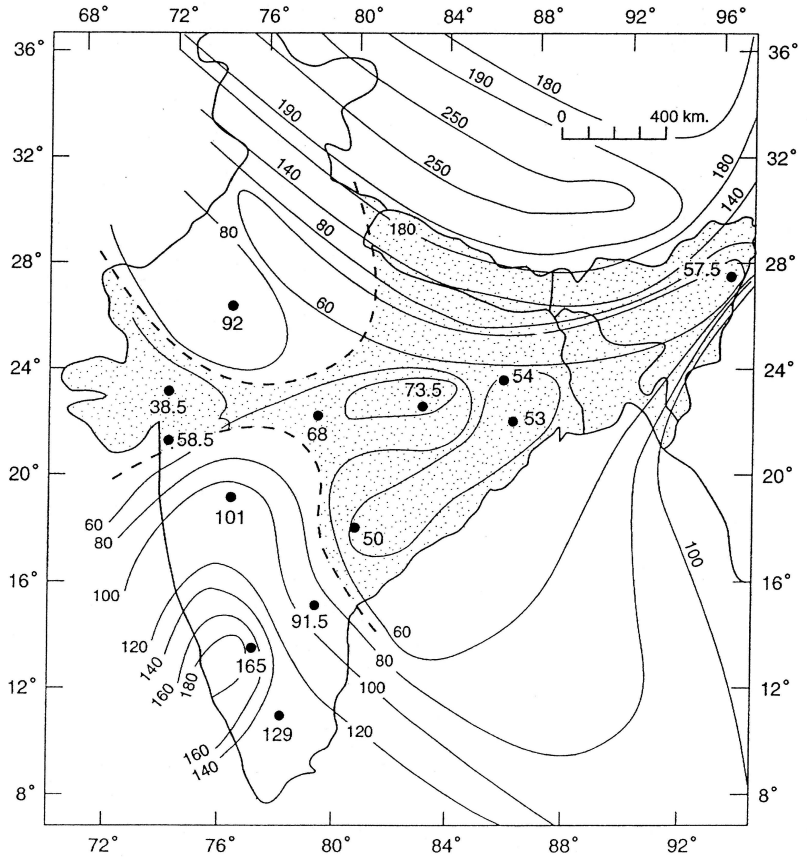

Fig.11a. Map of the lower boundary of the lithosphere (after Negi et al. (1986), Nedoma (1998a)).

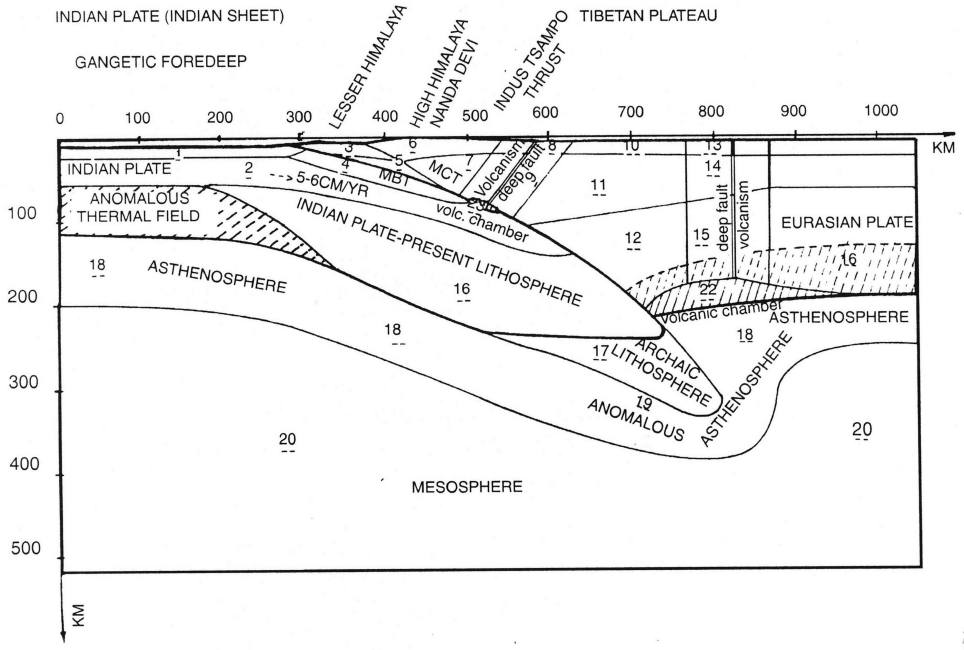

Fig.11b. Geodynamic model of Himalayas in the cross-section (after Nedoma (1998a,b)).

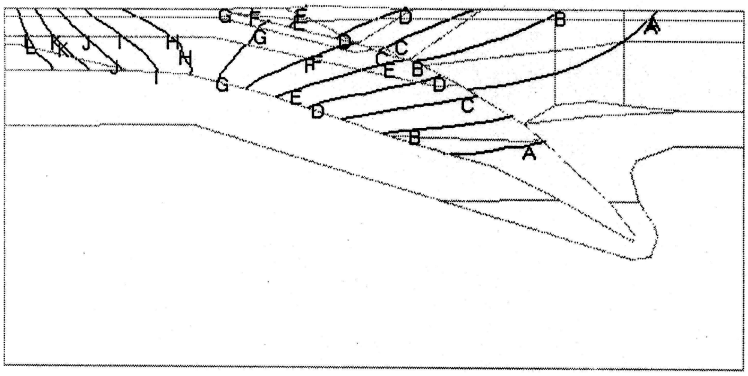

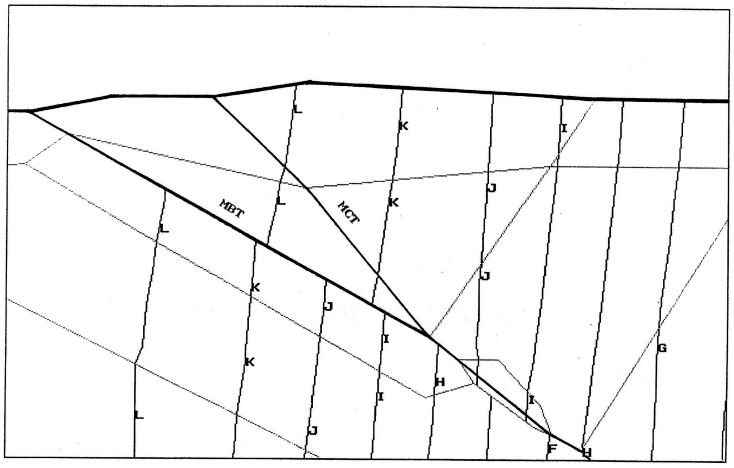

(b)

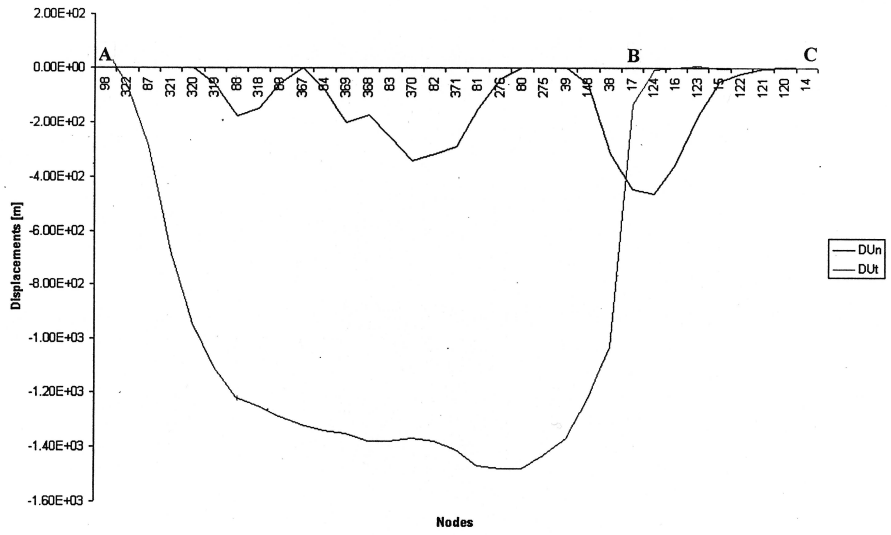

(c)

Figs 12a-c. Geodynamic model of Himalayas
(a) The rate of convergence in mm/yr $A = 3.84$, $B = 7.69$, $C = 11.53$, $D = 15.38$, $E = 19.22$, $F = 23.07$ $G = 26.92$, $H = 30.76$, $I = 34.61$, $J = 38.46$, $K = 42.30$, $L = 46.15$
(b) the rate of uplift in mm/yr $A = 0.8$, $B = 2.95$, $C = 5.11$, $D = 7.26$, $E = 9.41$, $F = 11.56$ $G = 13.72$, $H = 15.87$, $I = 18.02$, $J = 20.17$, $K = 22.32$, $L = 24.47$
(c) normal and tangential components of displacement vector on the contact boundary between the invasing Indian plate and the Eurasian plate (denoted as ABC) $(DUn, DUt\ [m/10^5 yrs])$.

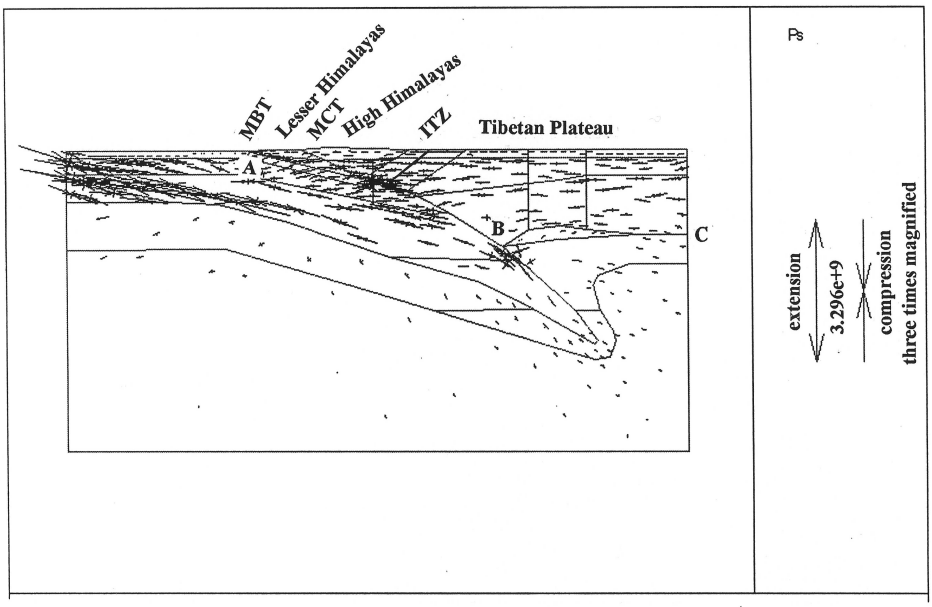

(a)

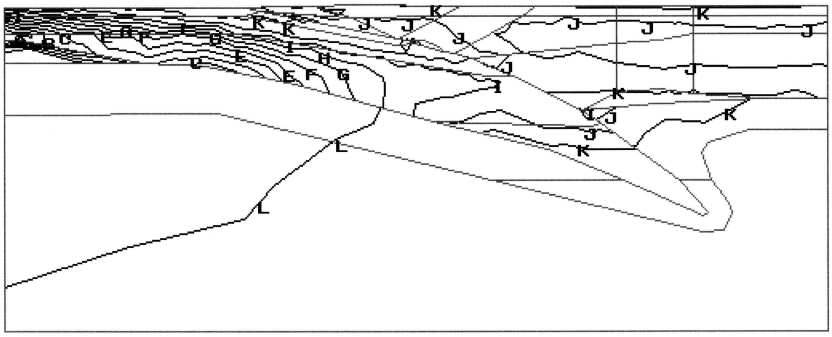

(b)

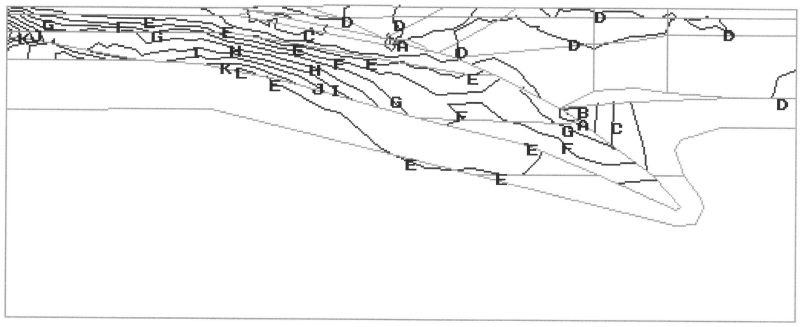

(c)

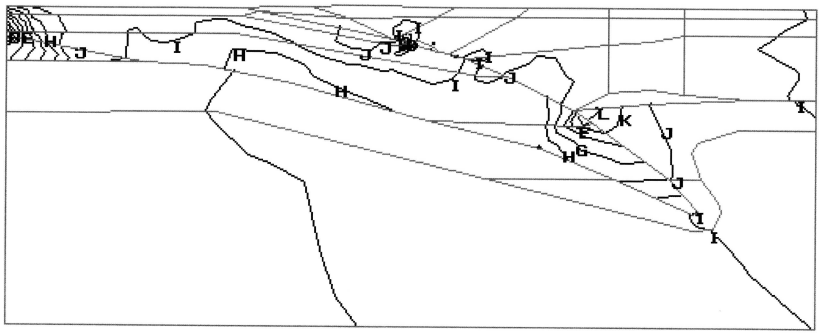

(d)

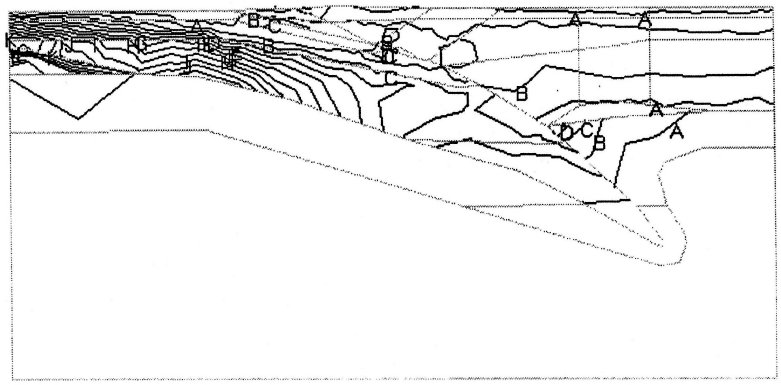

(e)

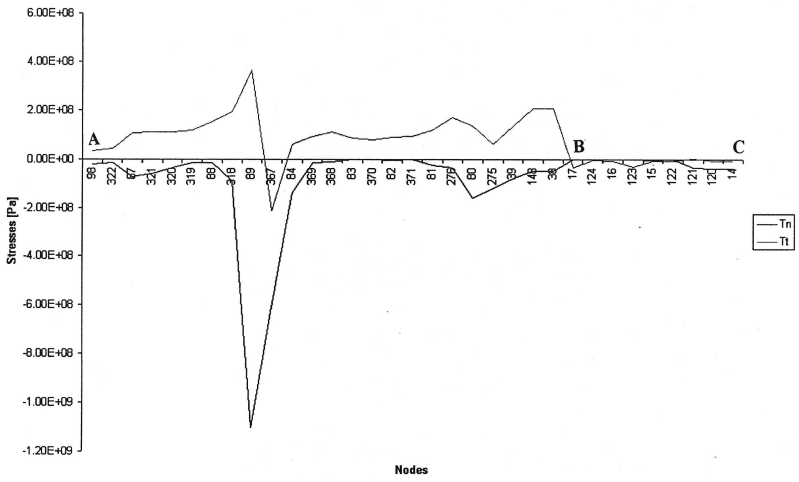
6.00E+08
4.00E+08
2.00E+08
0.00E+00
-2.00E+08
-4.00E+08
-6.00E+08
-8.00E+08
-1.00E+09
-1.20E+09
Stresses [Pa]
A
B
C
Nodes
Tn
Tt

(f)

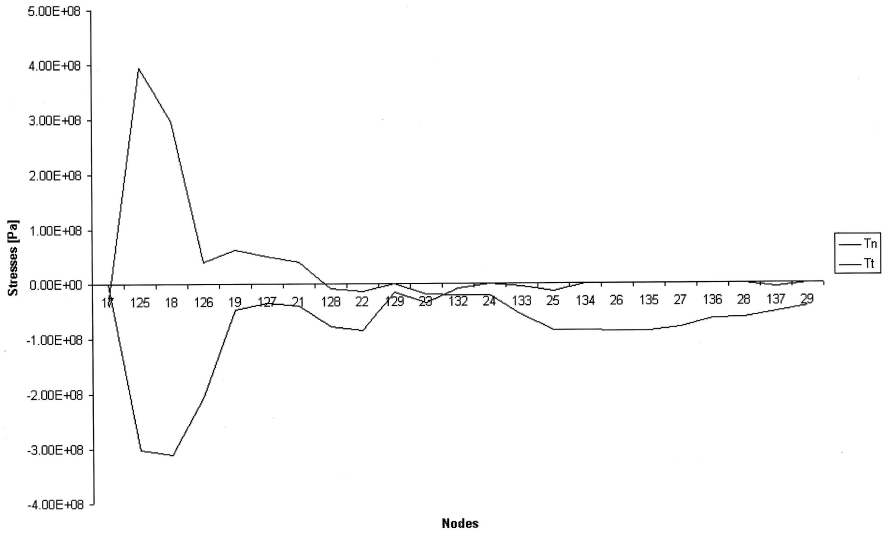

(g)

Fig. 13a-g. Geodynamic model of the Himalayas (after Nedoma (1998a,b)).
(a) Distribution of the principal stresses ($\max|3.296e+9|$ [MPa /1.2 $\cdot 10^5$ yrs], (corresponding to the rate ~ 0.02746 MPa/yr)
(b) the rate of horizontal stress component (S_x $[MPa/yr]$) $A = -0.017475$, $B = -0.01586$, $C = -0.014241$, $D = -0.012625$, $E = -0.01008$, $F = -0.009392$, $G = -0.00778$, $H = -0.006162$, $I = -0.00454$, $J = -0.00293$, $K = -0.00131$, $L = 0.0003$
(c) the rate of shear stress component (S_{xz} $[MPa/yr]$) $A = -0.00146$, $B = -0.00097$, $C = -0.00047$, $D = 0.000021$, $E = 0.00052$, $F = 0.00101$, $G = 0.00151$, $H = 0.0020$, $I = 0.00249$, $J = 0.00299$, $K = 0.003486131$, $L = 0.00398$
(d) the rate of vertical stress component (S_z $[MPa/yr]$) $A = -0.00461$, $B = -0.00407$, $C = -0.003525$, $D = -0.00298$, $E = -0.002437$, $F = -0.001892$, $G = -0.00135$, $H = -0.000804$, $I = -0.0002597$, $J = 0.000285$, $K = 0.000829$, $L = 0.00137$
(e) the rate of stress equivalent (S_e $[MPa/yr]$) $A = 0.0101397$, $B = 0.00263$, $C = 0.00386$, $D = 0.00597$, $E = 0.00633$, $F = 0.007565$, $G = 0.00879$, $H = 0.010025$, $I = 0.01126$, $J = 0.012492$, $K = 0.013725$, $L = 0.01496$
(f) normal and tangential components of stress vector on the contact boundary between the invasing Indian plate and the Eurasian plate (Tn, Tt $[MPa/1.2 \times 10^5 yrs]$) between points $(98, 17, 14) \equiv ABC$.
(g) normal and tangential components of stress vector on the contact boundary between the invasing Indian plate and the Eurasian plate (Tn, Tt $[MPa/1.2 \times 10^5 yrs]$) between points $(17, 24, 29)$.

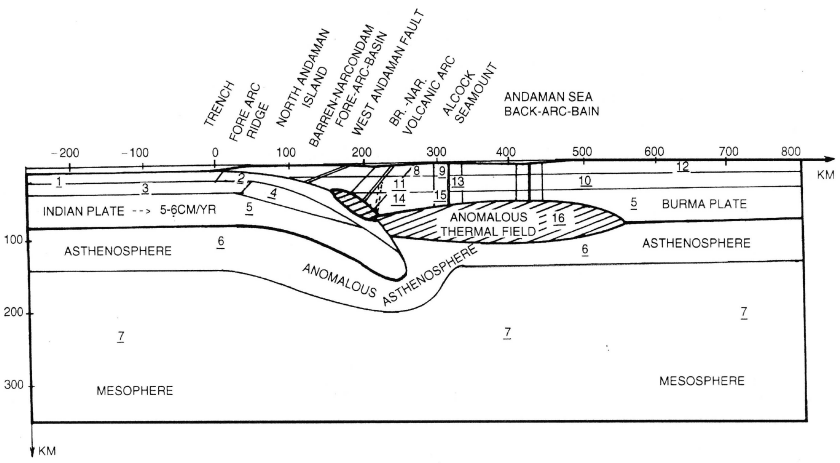

Fig. 14. Geodynamic model of the North Andaman Island Arc system in the cross-section (after Nedoma (1998a,b)).

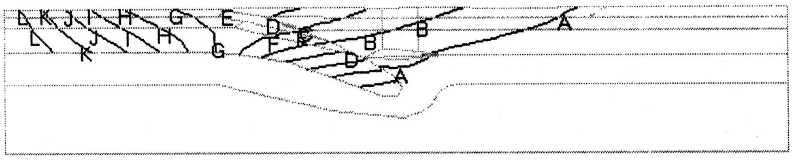

(a)

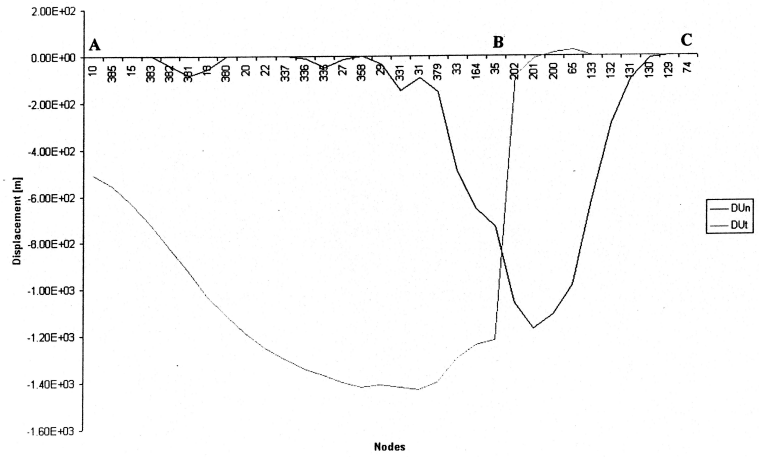

(b)

Fig. 15a,b. Geodynamic model of the North Andaman Island Arc system (after Nedoma (1998a,b)). (a) The rate of convergence in $[mm/yr]$ $A = 3.85$, $B = 7.692$, $C = 11.53$, $D = 15.38$, $E = 19.23$, $F = 23.07$, $G = 26.92$, $H = 30.77$, $I = 34.61$, $J = 38.46$, $K = 42.30$, $L = 46.15$.

(b) Normal and tangential components of displacement vector on the contact boundary between the invasing Indian plate and Burmese plate (denoted as ABC) (DUn, DUt $[m/10^5 yrs]$)

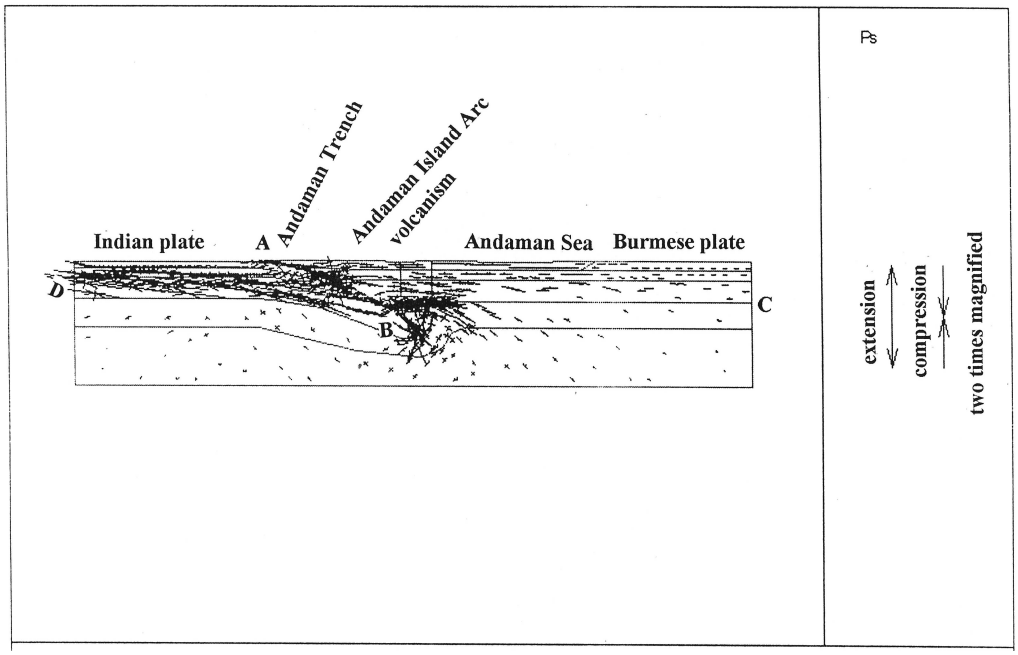
Ps
Andaman Trench
Andaman Island Arc
volcanism
Indian plate
A
Andaman Sea
Burmese plate
D
B
C
extension
compression
two times magnified

(a)

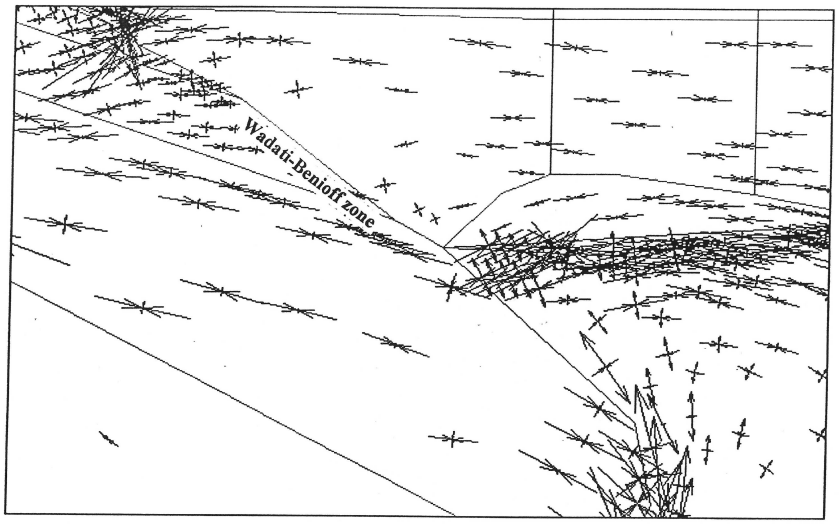
Wadati-Benioff zone

(b)

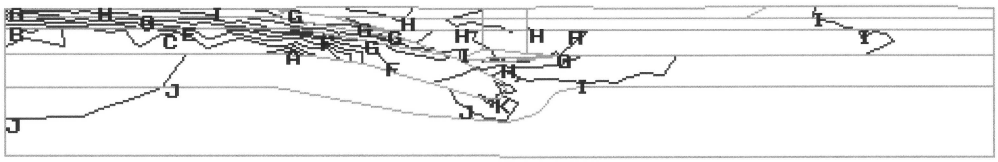

(c)

(d)

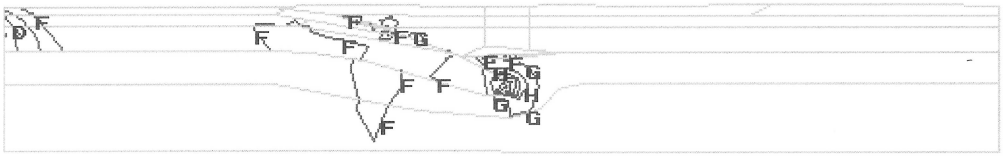

(e)

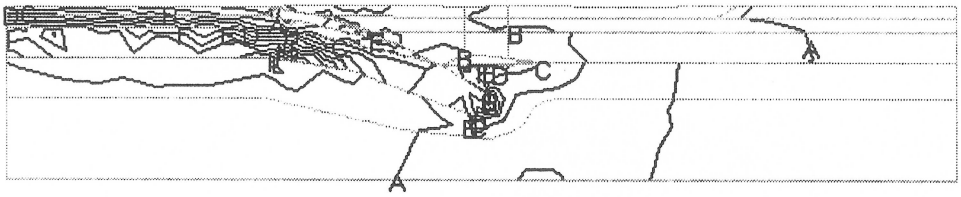

(f)

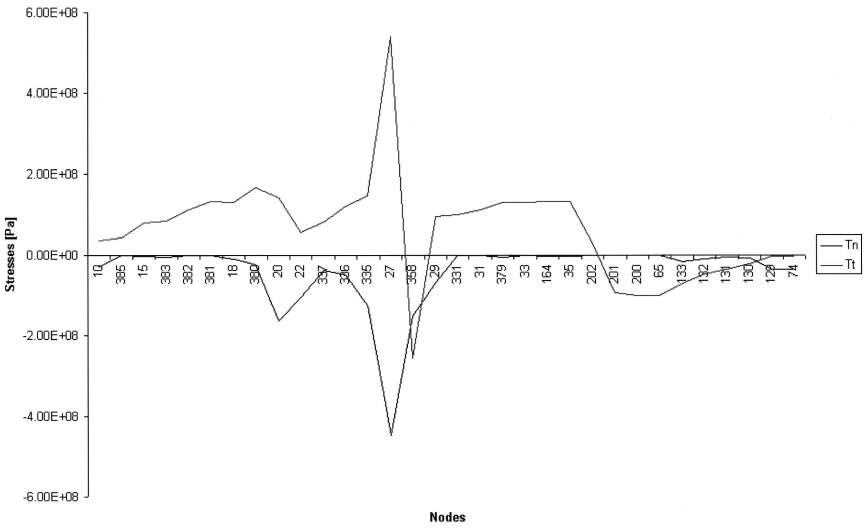

(g)

Fig. 16a-g. Geodynamic model of the North Andaman Island arc system (after Nedoma (1998a,b)).
(a) Distribution of the rate of principal stresses ($\max|0.02066|$ $[MPa/yr]$),
(b) distribution of the rate of principal stresses in the zoom region ($[MPa/yr]$),
(c) the rate of horizontal stress component (S_x $[MPa/yr]$) $A = -0.014166$, $B = -0.012533$, $C = -0.0109$, $D = -0.009266$, $E = -0.00764$, $F = -0.006$, $G = -0.00437$, $H = -0.00274$, $I = -0.00111$, $J = 0.00052$, $K = 0.00215$, $L = 0.00378$
(d) the rate of shear stress component (S_{xz} $[MPa/yr]$) $A = -0.00241$, $B = -0.00185$, $C = -0.00128$, $D = -0.00071$, $E = -0.00015$, $F = 0.00042$, $G = 0.000866$, $H = 0.0015533$, $I = 0.00212$, $J = 0.00269$, $K = 0.00325$, $L = 0.00382$
(e) the rate of vertical stress component (S_z $[MPa/yr]$) $A = -0.00619$, $B = -0.00504$, $C = -0.00388$, $D = -0.00273$, $E = -0.00157$, $F = -0.00042$, $G = 0.00073$, $H = 0.00189$, $I = 0.00304$, $J = 0.00419$, $K = 0.00535$, $L = 0.00650$
(f) the rate of stress equivalent (S_e $[MPa/yr]$) $A = 0.00115$, $B = 0.00228$, $C = 0.00342$, $D = 0.00455$, $E = 0.00057$, $F = 0.00682$, $G = 0.00796$, $H = 0.00909$, $I = 0.01022$, $J = 0.011358$, $K = 0.01249$, $L = 0.01362$
(g) normal and tangential components of stresses on the contact boundary between the invasing Indian plate and Burmese plate ($Tn, Tt[MPa/10^5 yrs]$).